APPROXIMATE METHODS FOR OBTAINING A ONE-GROUP NODAL SOLUTION WITH TWO-GROUP PARAMETERS

by

BRUCE WILLIAM HAGEMEIER
B.S., University of California, Los Angeles
(1981)

SUBMITTED TO THE DEPARTMENT OF NUCLEAR ENGINEERING IN PARTIAL FULFILLMENT OF THE REQUIREMENTS FOR THE DEGREE OF MASTER OF SCIENCE

at the

MASSACHUSETTS INSTITUTE OF TECHNOLOGY

August 1982

Signature of Author: .....
Department of Nuclear Engineering
August 28, 1982

Certified by: .....
Allan F. Henry
Thesis Supervisor

Accepted by: .....
Allan F. Henry
Chairman, Departmental Graduate Committee

APPROXIMATE METHODS FOR OBTAINING A ONE-GROUP NODAL SOLUTION WITH TWO-GROUP PARAMETERS

by

Bruce William Hagemeier

Submitted to the Department of Nuclear Engineering on August 28, 1982, in partial fulfillment of the requirements for the degree of Master of Science in the field of Nuclear Engineering.

ABSTRACT

A method of obtaining approximate one-group equivalent diffusion theory parameters and discontinuity factors for use in the nodal code QUANDRY was developed. These approximate one-group quantities were determined from the two-group reference cross sections by performing assembly calculations with albedo boundary conditions.

An approximate one-group solution was obtained with this method for two different reactors: EPRI-9, which models a simplified PWR core, and CISE, which models a simplified BWR core. The accuracy of these approximate solutions was excellent. For EPRI-9, the reactor eigenvalue was predicted to within 0.03% and the maximum error in node averaged reaction rates was 0.99%. For CISE, the reactor eigenvalue was predicted to within 0.02% and the maximum error in node averaged reaction rates was 2.8%.

When compared to the two-group solutions obtained using the identical approximations, the one-group solution was found to be more accurate. The superior performance in one-group was attributed to the fact that, near the reflector, QUANDRY approximated the transverse leakage shape more accurately in one group than in two groups.

Thesis Supervisor: Allan F. Henry

Title: Professor of Nuclear Engineering

TABLE OF CONTENTS

TABLE OF CONTENTS (continued)

ACKNOWLEDGEMENTS

I consider myself fortunate to have had Professor Allan F. Henry as my thesis supervisor. His knowledge of reactor physics and his gift for teaching have made my association with him an extremely rewarding experience.

I am also indebted to my office-mates, Philippe Finck, Hussein Khalil, and Kent Parsons for their generous assistance during the course of this investigation. I hope we have the opportunity to work together again in the future.

Thanks also to Professor Michael J. Driscoll, who served as reader for this thesis, and to Ms. Delphine Radcliffe for her skill and patience in typing the final manuscript.

Finally, I would like to thank Susan Clifford for her support and understanding. She has made this past year the happiest time of my life.

LIST OF FIGURES

LIST OF TABLES

LIST OF TABLES (continued)

LIST OF TABLES (continued)

LIST OF TABLES (continued)

CHAPTER 1

INTRODUCTION

1.1 Introduction

Finite difference methods have been the workhorse of the nuclear industry for the past two decades. Such methods provide detailed multi-dimensional power distributions at an affordable cost when compared to other methods such as continuous energy Monte Carlo or multigroup discrete ordinates. That is not to say, however, that finite difference methods are cheap. To analyze a typical PWR in three dimensions having millions of mesh points requires hours of CPU time on the largest of digital computers.[1]

For many phases of reactor design and development, the detailed multi-dimensional power distribution obtained with finite difference methods is not needed. For example, many thermal hydraulic analyses, transient safety analyses and reload analyses often require only assembly averaged powers and the reactor eigenvalue. Clearly, it is a waste of time and effort to determine the detailed multi-dimensional power distribution only to integrate out the average quantities of interest.

In an attempt to eliminate this waste, the past few years have seen the development of various nodal methods. The great advantage with nodal methods is the relatively small number of unknowns resulting from the use of large, assembly-sized mesh intervals. Assuming the nodal equations are not too complex, the reduction in the number of unknowns translates directly into a reduction in computational effort.

The nodal code currently in use at MIT is QUANDRY.[1,2] Depending upon the size of the problem being analyzed, QUANDRY is from 10 to 1000 times[3] more computationally efficient than finite

difference codes. In addition, the accuracy of QUANDRY is at least as good as with finite difference codes. However, QUANDRY also has some drawbacks. QUANDRY cannot be readily extended beyond two energy groups and requires a great deal of computer memory capacity. For large two and three dimensional problems, the required computer memory capacity is excessive. Both these drawbacks could be mitigated if a suitable group collapsing procedure were found.

The goal of this thesis is to develop a suitable group collapsing procedure for use with the nodal code QUANDRY. Such a procedure would permit a three or four group problem to be collapsed to two groups, thereby allowing the problem to be analyzed with QUANDRY. Such a procedure would also permit a two-group problem to be collapsed to one-group, thereby cutting the required computer memory capacity in half.

1.2 The QUANDRY Equations

To derive the QUANDRY equations, one may begin with the Boltzmann transport equation. Integrating over all directions $\underline{\Omega}$ and an energy range ΔE_g reduces the transport equation to

$$\nabla \cdot \underline{J}_g(\underline{r}) + \Sigma_{t_g}(\underline{r})\,\varphi_g(\underline{r}) = \sum_{g'=1}^{2} \left[\Sigma_{gg'}(\underline{r}) + \frac{1}{\lambda}\,\chi_g\,\nu\Sigma_{f_{g'}} \right] \varphi_{g'}(\underline{r}) ; \qquad g = 1, 2 \tag{1-1}$$

where

$$\varphi_g(\underline{r}) \equiv \int d\Omega \int_{\Delta E_g} dE\ \psi(\underline{r}, \underline{\Omega}, E)$$

$$\underline{J}_g(\underline{r}) \equiv \int d\Omega \int_{\Delta E_g} dE\ \underline{\Omega}\,\psi(\underline{r}, \underline{\Omega}, E)$$

$$\Sigma_{\alpha_g}(\underline{r}) \equiv \frac{\int d\Omega \int_{\Delta E_g} dE \; \Sigma_\alpha(\underline{r}, E)\, \psi(\underline{r}, \underline{\Omega}, E)}{\varphi_g(\underline{r})}; \quad \alpha = t, f$$

$$\Sigma_{gg'}(\underline{r}) \equiv \frac{\int d\Omega \int_{\Delta E_g} dE \int_{\Delta E_{g'}} dE' \; \Sigma_{s_o}(\underline{r}, E' \to E)\, \psi(\underline{r}, \underline{\Omega}, E')}{\varphi_{g'}(r)}$$

$$\chi_g \equiv \int_{\Delta E_g} dE \; f(E)$$

Note that the presence of more than one fissionable isotope has been suppressed.

Next, Equation (1-1) is integrated over the volume of an arbitrary node (i, j, k), yielding

$$h_y^j h_z^k \left(\bar{J}_{g_x}^{(i,j,k)}(x_{i+1}) - \bar{J}_g^{(i,j,k)}(x_i) \right) + h_x^i h_z^k \left(\bar{J}_{g_y}^{(i,j,k)}(y_{j+1}) \right.$$

$$\left. - \bar{J}_{g_y}^{(i,j,k)}(y_j) \right) + h_x^i h_y^j \left(\bar{J}_{g_z}^{(i,j,k)}(z_{k+1}) - \bar{J}_{g_z}^{(i,j,k)}(z_k) \right)$$

$$+ h_x^i h_y^j h_z^k \, \bar{\Sigma}_{t_g}^{(i,j,k)} \, \bar{\bar{\varphi}}_g^{(i,j,k)} = \sum_{g'=1}^{2} h_x^i h_y^j h_z^k$$

$$\left(\bar{\Sigma}_{gg'}^{(i,j,k)} + \frac{1}{\lambda} \chi_g \nu \bar{\Sigma}_{f_{g'}}^{(i,j,k)} \right) \bar{\bar{\varphi}}_{g'}^{(i,j,k)} \qquad (1\text{-}2)$$

where

$$\bar{\bar{\varphi}}_g^{(i,j,k)} \equiv \frac{1}{h_x^i h_y^j h_z^k} \int_{h_x^i} dx \int_{h_y^j} dy \int_{h_z^k} dz \; \varphi_g(x, y, z)$$

$$\bar{J}_{g_u}^{(\ell, m, n)}(u_\ell) \equiv \frac{1}{h_v^m h_w^n} \int_{v_m} dv \int_{w_n} dw\, J_g(u_\ell, v, w)$$

$$\bar{\Sigma}_\alpha^{(i, j, k)} \equiv \frac{\int_{h_x^i} dx \int_{h_y^j} dy \int_{h_z^k} dz\ \Sigma_{\alpha g'}(x, y, z)\, \varphi_{g'}(x, y, z)}{h_x^i h_y^j h_z^k \bar{\varphi}_{g'}^{(i, j, k)}}; \quad \alpha = t, f, g$$

In the above definitions, a generalized notation has been introduced:

$u \equiv$ x, y, or z

$v \equiv$ x, y, or z; $u \neq v$

$w \equiv$ x, y, or z; $u \neq v \neq w$

$\ell \equiv$ i, j, or k

$m \equiv$ i, j, or k; $\ell \neq m$

$n \equiv$ i, j, or k; $\ell \neq m \neq n$

Thus, $\bar{J}_{g_u}^{(i, j, k)}(u)$ actually defines the surface averaged net current in the x, y and z directions.

There is no theoretical reason why the QUANDRY equations cannot be derived using a non-Cartesian coordinate system. However, since most reactors lend themselves to analysis with rectangular or cubical nodes, QUANDRY was limited to Cartesian geometry.

Equation (1-2) is a formally exact neutron balance for node (i, j, k). But before this equation can be solved, additional relationships must be found between the node averaged flux and surface averaged net currents. Specifically, six coupling equations are required for three dimensions.

Many different schemes have been examined for determining

coupling equations. In earlier schemes, crude approximations limited the accuracy of nodal methods. More recently, coupling equations have been determined using relatively mild approximations. Consequently, the accuracy of nodal methods has improved dramatically. As always, though, nothing is free; the coupling equations used in QUANDRY are extremely complex algebraically. While these coupling equations are not explicitly derived in this thesis, a sketch of their derivation is presented below. An explicit derivation is given in Reference 4.

The QUANDRY coupling equations may be determined beginning with Equation (1-1). To determine the coupling equations in the u direction, we assume that the net current in the u direction can be represented by Fick's law

$$\bar{J}_{g_u}^{(i,j,k)}(u) = -\frac{1}{h_v^m h_w^n}\int_{h_v^m} dv \int_{h_w^n} dw\, \bar{D}_g^{(i,j,k)} \frac{\partial}{\partial u}\, \varphi_g\,(u,v,w) \tag{1-3}$$

The definition of the homogenized group-g diffusion coefficient will be discussed later. Now, integrating Equation (1-1) over the two directions transverse to the u direction and substituting for Fick's law yields

$$- h_v^m\, h_w^n\, \bar{D}_{g_u}^{(\ell,m,n)} \frac{\partial^2}{\partial u^2}\, \bar{\varphi}_{g_u}^{(\ell,m,n)}(u) + h_w^n\, L_{g_v}^{(\ell,m,n)}(u)$$

$$+ h_v^m\, L_{g_w}^{(\ell,m,n)}(u) + h_v^m\, h_w^n\, \bar{\Sigma}_{t_g}^{(\ell,m,n)}\, \bar{\varphi}_{g_u}^{(\ell,m,n)}(u)$$

$$= \sum_{g'=1}^{2} h_v^m\, h_w^n \left(\bar{\Sigma}_{gg'}^{(\ell,m,n)} + \chi_g \nu \bar{\Sigma}_{f_{g'}}^{(\ell,m,n)}\right) \bar{\varphi}_{g'_u}^{(\ell,m,n)}(u) \tag{1-4}$$

where

$$\bar{\varphi}_{g_u}^{(\ell, m, n)}(u) \equiv \frac{1}{h_v^m h_w^n} \int_{v_m}^{v_{m+1}} dv \int_{w_n}^{w_{n+1}} dw\, \varphi_g(u, v, w)$$

$$L_{g_v}^{(\ell, m, n)}(u) \equiv \bar{J}_{g_v}^{(\ell, m, n)}(u, v_{m+1}) - \bar{J}_{g_v}^{(\ell, m, n)}(u, v_m)$$

If we introduce a transverse leakage term

$$S_{g_u}^{(\ell, m, n)}(u) \equiv \frac{1}{h_v^m} L_{g_v}^{(\ell, m, n)}(u) + \frac{1}{h_w^n} L_{g_w}^{(\ell, m, n)}(u) \tag{1-5}$$

and divide through by $h_v^m\, h_w^n$, Equation (1-4) becomes

$$- \bar{D}_{g_u}^{(\ell, m, n)} \frac{\partial^2}{\partial u^2} \bar{\varphi}_{g_u}^{(\ell, m, n)}(u) + \bar{\Sigma}_{t_g}^{(\ell, m, n)} \bar{\varphi}_g^{(\ell, m, n)}(u) - \sum_{g'=1}^{2} \left(\bar{\Sigma}_{gg'}^{(\ell, m, n)} + \chi_g \nu \bar{\Sigma}_{f_{g'}}^{(\ell, m, n)} \right) \bar{\varphi}_{g'}^{(\ell, m, n)}(u) = - S_{g_u}^{(\ell, m, n)}(u) \tag{1-6}$$

If the transverse leakage term $S_{g_u}^{(\ell, m, n)}(u)$ were known, integration of Equation (1-6) would yield directly the first two coupling equations. Similar equations for the v and w directions would yield the other four coupling equations. Together with Equations (1-2) and the appropriate set of boundary conditions, these six coupling equations would form a well-posed problem which could be solved numerically. Unfortunately, the transverse leakages are not known, necessitating the first and only approximation in QUANDRY whereby $S_{g_u}^{(\ell, m, n)}(u)$ is fit to a quadratic function of u over nodes $(\ell-1, m, n)$, (ℓ, m, n) and $(\ell+1, m, n)$. The coefficients of the quadratic function are determined by requiring that the correct surface averaged transverse leakages be preserved for each of the three adjacent nodes.

With $S_{g_u}^{(\ell, m, n)}(u)$ approximated by a quadratic, Equation (1-6) can be solved for $\bar{\varphi}_{g_u}^{(\ell, m, n)}(u)$ within node (ℓ, m, n) using $\bar{J}_{g_u}^{(\ell, m, n)}(u_\ell)$ and $\bar{\varphi}_{g_u}^{(\ell, m, n)}(u_\ell)$ as boundary conditions. Integration of the solution $\bar{\varphi}_{g_u}^{(\ell, m, n)}(u)$ over h_u^ℓ then yields a complex algebraic function relating the surface averaged flux $\bar{\varphi}_{g_u}^{(\ell, m, n)}(u_\ell)$ to the surface averaged net current $\bar{J}_{g_u}^{(\ell, m, n)}(u_\ell)$ and the three surface averaged transverse leakages:

$$\bar{\varphi}_{g_u}^{(\ell, m, n)}(u_\ell) = f^{(\ell)}\left(\bar{J}_{g_u}^{(\ell, m, n)}(u_\ell), \bar{\bar{\varphi}}_{g}^{(\ell, m, n)}, \bar{S}_{g_u}^{(\ell-1, m, n)}, \bar{S}_{g_u}^{(\ell, m, n)}, \bar{S}_{g_u}^{(\ell+1, m, n)}\right) \tag{1-7}$$

Here,

$$\bar{S}_{g_u}^{(\ell, m, n)} \equiv \frac{1}{h_u^\ell} \int_{h_u^\ell}^{h_u^{\ell+1}} S_{g_u}^{(\ell, m, n)}(u)$$

Equation (1-7) couples the surface averaged net current to the node averaged flux. However, the direct use of Equation (1-7) as a coupling equation is precluded by the presence of a new unknown: $\bar{\varphi}_{g_u}^{(i, j, k)}(u_\ell)$, the surface averaged flux. To eliminate this unknown, Equation (1-6) is solved within the adjacent node $(\ell-1, m, n)$ using $\bar{\varphi}_{g_u}^{(\ell-1, m, n)}(u_\ell)$ and $\bar{J}_{g_u}^{(\ell-1, m, n)}(u_\ell)$ as boundary conditions. Integrating the solution $\bar{\varphi}_{g_u}^{(\ell-1, m, n)}(u)$ over $h_u^{\ell-1}$ then yields an equation whose form is identical to that of Equation (1-7):

$$\bar{\varphi}_{g_u}^{(\ell-1, m, n)}(u_\ell) = g^{(\ell)}\left(\bar{J}_{g_u}^{(\ell-1, m, n)}(u_\ell), \bar{\bar{\varphi}}_{g}^{(\ell, m, n)}, \bar{S}_{g_u}^{(\ell-2, m, n)}, \bar{S}_{g_u}^{(\ell-1, m, n)}, \bar{S}_{g_u}^{(\ell, m, n)}\right) \tag{1-8}$$

Equations (1-7) and (1-8) may now be combined to eliminate $\bar{\varphi}_{g_u}^{(\ell, m, n)}(u_\ell)$ and $\bar{\varphi}_{g_u}^{(\ell-1, m, n)}(u_\ell)$ by assuming, for the moment, that the surface averaged flux and net current are continuous across nodal boundaries

$$\bar{\varphi}_{g_u}^{(\ell-1, m, n)}(u_\ell) = \bar{\varphi}_{g_u}^{(\ell, m, n)}(u_\ell) \tag{1-9}$$

$$\bar{J}_{g_u}^{(\ell-1, m, n)}(u_\ell) = \bar{J}_{g_u}^{(\ell, m, n)}(u_\ell) \tag{1-10}$$

Thus, the desired coupling equation has the form

$$\bar{J}_{g_u}^{(\ell, m, n)}(u_\ell) = h^{(\ell)}\left(\bar{\bar{\varphi}}_{g_u}^{(\ell-1, m, n)}, \bar{\bar{\varphi}}_{g_u}^{(\ell, m, n)}, \bar{S}_{g_u}^{(\ell-2, m, n)}, \bar{S}_{g_u}^{(\ell-1, m, n)}, \bar{S}_{g_u}^{(\ell, m, n)}, \bar{S}_{g_u}^{(\ell+1, m, n)}\right) \tag{1-11}$$

Equation (1-11) is an involved algebraic function relating the surface averaged net current to two adjacent node averaged fluxes and four adjacent surface averaged transverse leakages. By following an identical procedure for nodes (ℓ, m, n) and $(\ell+1, m, n)$, a similar coupling equation can be obtained for $\bar{J}_{g_u}^{(\ell, m, n)}(u_{\ell+1})$

$$J_{g_u}^{(\ell, m, n)}(u_{\ell+1}) = h^{(\ell+1)}\left(\bar{\bar{\varphi}}^{(\ell, m, n)}, \bar{\bar{\varphi}}^{(\ell+1, m, n)}, \bar{S}_{g_u}^{(\ell-1, m, n)}, \bar{S}_{g_u}^{(\ell, m, n)}, \bar{S}_{g_u}^{(\ell+1, m, n)}, \bar{S}_{g_u}^{(\ell+2, m, n)}\right) \tag{1-12}$$

Equations (1-2), (1-11) and (1-12) constitute the QUANDRY equations. The actual strategy whereby these equations are solved on a

digital computer will not be discussed in this thesis. A detailed account of the numerical techniques used to solve these equations is given in Reference 4.

1.3 Discontinuity Factors

Actually, the assumption of Equation (1-9) that the surface averaged flux is continuous across nodal boundaries leads to error.[2] To illustrate this, consider a heterogeneous one-dimensional node and the identical node after homogenization. To further simplify matters, suppose the neutron flux within each of these nodes can be adequately described with one-group diffusion theory. For the heterogeneous node

$$-\frac{\delta}{\delta u} D(u) \frac{\delta}{\delta u} \varphi(u) + \Sigma_a(u) \varphi(u) = \frac{1}{\lambda} \nu \Sigma_f(u) \varphi(u) , \qquad (1\text{-}13)$$

while for the homogenized node

$$-\bar{D} \frac{\delta^2}{\partial u^2} \bar{\varphi}(u) + \bar{\Sigma}_a \bar{\varphi}(u) = \frac{1}{\lambda} \nu \bar{\Sigma}_f \bar{\varphi}(u) \qquad (1\text{-}14)$$

where

$$\bar{\Sigma}_\alpha \equiv \frac{\int_{h_u} du \; \Sigma_\alpha(u) \varphi(u)}{\int_{h_u} du \; \bar{\varphi}(u)} ; \quad \alpha = a, f$$

For the moment the homogenized diffusion coefficient will be defined only as some position independent number.

We wish the solution of the homogenized problem to preserve the heterogeneous eigenvalue. In addition, the one-group homogenized cross sections have been defined such that the node averaged reaction rates are preserved. Now, if we integrate Equations (1-13) and (1-14) over h_u and rearrange, we obtain:

$$\left\{\left[D(u)\frac{\partial}{\partial u}\varphi(u)\right]_{u_{\ell+1}} - \left[D(u)\frac{\partial}{\partial u}\varphi(u)\right]_{u_\ell}\right\}$$

$$= \left\{\left[\overline{D}\frac{\partial}{\partial u}\varphi(u)\right]_{u_{\ell+1}} - \left[\overline{D}\frac{\partial}{\partial u}\bar{\varphi}(u)\right]_{u_\ell}\right\} \qquad (1\text{-}15)$$

In other words, preserving the reactor eigenvalue and node averaged reaction rates implies that the net nodal leakage rate is also preserved.

The individual surface currents are measurable quantities and should be preserved on physical grounds. However, if these net surface currents are taken as boundary conditions and used to solve Equations (1-13) and (1-14), one finds that the homogeneous surface flux does not, in general, equal the heterogeneous surface flux.

While this fact may seem strange at first, it makes perfect sense. The homogenized problem is an artificial mathematical problem, constructed so that certain node averaged quantities are preserved. The homogenized problem does not preserve the heterogeneous flux profile. Thus, while the heterogeneous flux is a physical quantity which is continuous across nodal boundaries, there is no reason why the homogeneous flux must also be continuous across nodal boundaries. In general, the homogeneous flux will be discontinuous across nodal boundaries.

At this point, the homogenized diffusion coefficient remains to be determined. In fact, the preservation of the node averaged reaction rates, surface averaged net currents and reactor eigenvalue will not depend on the means by which the diffusion coefficient is homogenized. Changing the value of $\overline{D}$ only affects the magnitude of the difference

between the heterogeneous surface flux and the homogeneous surface flux. Thus, the diffusion coefficient can be homogenized in the most straightforward manner, usually by simply flux weighting D(u):

$$\overline{D} \equiv \frac{\int_{h_u} du\, D(u)\, \varphi(u)}{\int_{h_u} du\, \bar{\varphi}(u)} \tag{1-16}$$

To relate the homogeneous surface flux across nodal boundaries, Kord Smith, modifying the work of Koebke, introduced "discontinuity factors"[2, 4]

$$f_{g_u}^{(\ell, m, n)}(u_{\ell+1}) \equiv \frac{\varphi_{g_u}^{(\ell, m, n)}(u_{\ell+1})}{\bar{\varphi}_{g_u}^{(\ell, m, n)}(u_{\ell+1})} \tag{1-17}$$

$$f_{g_u}^{(\ell, m, n)}(u_{\ell}) \equiv \frac{\varphi_{g_u}^{(\ell, m, n)}(u_{\ell})}{\bar{\varphi}_{g_u}^{(\ell, m, n)}(u_{\ell})} \tag{1-18}$$

Here, discontinuity factors are defined as the ratio of the surface averaged heterogeneous flux to the surface averaged homogeneous flux. From these definitions the relationship between the surface averaged homogeneous flux for adjacent nodes is

$$f_{g_u}^{(\ell, m, n)}(u_{\ell})\, \bar{\varphi}_{g_u}^{(\ell, m, n)}(u_{\ell}) = f_{g_u}^{(\ell-1, m, n)}(u_{\ell})\, \bar{\varphi}_{g_u}^{(\ell-1, m, n)}(u_{\ell}) \tag{1-19}$$

When used to relate the surface averaged flux of adjacent nodes, Eq. (1-19) allows the QUANDRY equations the necessary degrees of freedom

required to reproduce the exact reactor eigenvalue, the exact node averaged reaction rates, and the exact surface averaged net currents.

Discontinuity factors may also be introduced to reproduce the exact solution when energy groups are collapsed. To illustrate this fact, consider a one-dimensional homogeneous node. If we assume that the flux profile may be adequately described by the continuous energy diffusion equation

$$-\frac{d}{du} D(E) \frac{d}{du} \varphi(u,E) + \Sigma_t(E) \varphi(u,E)$$

$$= \int_0^\infty dE' \left[\Sigma_s(E' \to E) + \frac{1}{\lambda} f(E) \nu\Sigma_f(E')\right] \varphi(u,E') \qquad (1\text{-}20)$$

collapsing to one group yields

$$-\frac{d^2}{du^2} (\hat{D}(u)\hat{\varphi}(u)) + (\hat{\Sigma}_t(u) - \hat{\Sigma}_s(u)) \hat{\varphi}(u) = \frac{1}{\lambda} \nu\hat{\Sigma}_f(u) \hat{\varphi}(u) \qquad (1\text{-}21)$$

where

$$\hat{\Sigma}_\alpha(u) \equiv \frac{\int_0^\infty dE \ \Sigma_\alpha(E) \varphi(u,E)}{\int_0^\infty dE \ \varphi(u,E)} ; \quad \alpha = s, t, f$$

$$\hat{\varphi}(u) \equiv \int_0^\infty dE \ \varphi(u,E)$$

$$\hat{D}(u) \equiv \frac{\int_0^\infty dE \ D(E) \varphi(u,E)}{\int_0^\infty dE \ \varphi(u,E)}$$

Notice that the one-group diffusion theory parameters are position dependent, though the node is homogeneous. This will be the case so long as

the neutron spectrum in the node, whose shape is given by $\varphi(u, E)$, is not asymptotic.

The QUANDRY equations may only be applied to homogeneous nodes. Therefore, the collapsed one-group diffusion parameters must be homogenized. The corresponding one-group diffusion equation for this homogenized node is

$$-\bar{D}\frac{d^2}{du^2}\bar{\phi}(u) + (\bar{\Sigma}_t - \bar{\Sigma}_s)\bar{\phi}(u) = \frac{1}{\lambda}\nu\bar{\Sigma}_f\bar{\phi}(u) \qquad (1\text{-}22)$$

where

$$\bar{\Sigma}_\alpha \equiv \frac{\int_{h_u} du\ \hat{\Sigma}_\alpha(u)\hat{\phi}(u)}{\int_{h_u} du\ \bar{\phi}(u)}\ ; \quad \alpha = s, t, f$$

$$\bar{D} \equiv \frac{\int_{h_u} du\ \hat{D}(u)\hat{\phi}(u)}{\int_{h_u} du\ \bar{\phi}(u)}$$

Now, Equations (1-21) and (1-22) may be compared using the earlier analysis of heterogeneous nodes. The same conclusion will be reached; that is, discontinuity factors are required to introduce sufficient degrees of freedom such that the reactor eigenvalue, node averaged reaction rates and surface averaged net currents can be preserved.

In these simple one-dimensional illustrations, the necessity of discontinuity factors is apparent. Now, the question arises as to whether or not the exact solution can still be reproduced in two dimensions when the transverse leakage term is approximated by a quadratic. Intuitively, one might feel that by approximating the transverse leakage term in the QUANDRY equations, some error must be introduced into

the final solution. However, this is not the case! One of the subtler implications of the use of discontinuity factors is that they allow an exact solution of the global problem to be obtained even though the QUANDRY equations are solved in an approximate manner. The only requirement is that the approximation used to obtain discontinuity factors also be used when solving the QUANDRY equations for the global problem.

1.4 QUANDRY Boundary Conditions

QUANDRY allows three boundary conditions: zero flux, zero current, and albedos. To sketch how QUANDRY incorporates these boundary conditions into its nodal equations, consider Node (ℓ, m) on the reactor periphery as shown in Fig. 1-1. The coupling equation for the $u_{\ell+1}$ face of Node (ℓ, m) is given by Equation (1-8):

$$\bar{\varphi}_g^{(\ell,m)}(u_{\ell+1}) = g^{(\ell)}\left(\bar{J}_{g_u}^{(\ell,m)}(u_{\ell+1}), \bar{\bar{\varphi}}_g^{(\ell,m)}, \bar{S}_{g_u}^{(\ell-1,m)}, \bar{S}_{g_u}^{(\ell,m)}, \bar{S}_{g_u}^{(\ell+1,m)}\right) \quad (1\text{-}8)$$

The surface flux $\bar{\varphi}_g^{(\ell,m)}$ is eliminated from this equation with either the zero flux or albedo boundary conditions. In either case, the resulting coupling equation assumes the form

$$\bar{J}_{g_u}^{(\ell,m)}(u_{\ell+1}) = i^{(\ell)}\left(\bar{\bar{\varphi}}_g^{(\ell,m)}, \bar{S}_g^{(\ell-1,m)}, S_{g_u}^{(\ell,m)}, \bar{S}_{g_u}^{(\ell+1,m)}\right) \quad (1\text{-}23)$$

With the zero current boundary condition, Equation (1-23) simply reduces to the identity

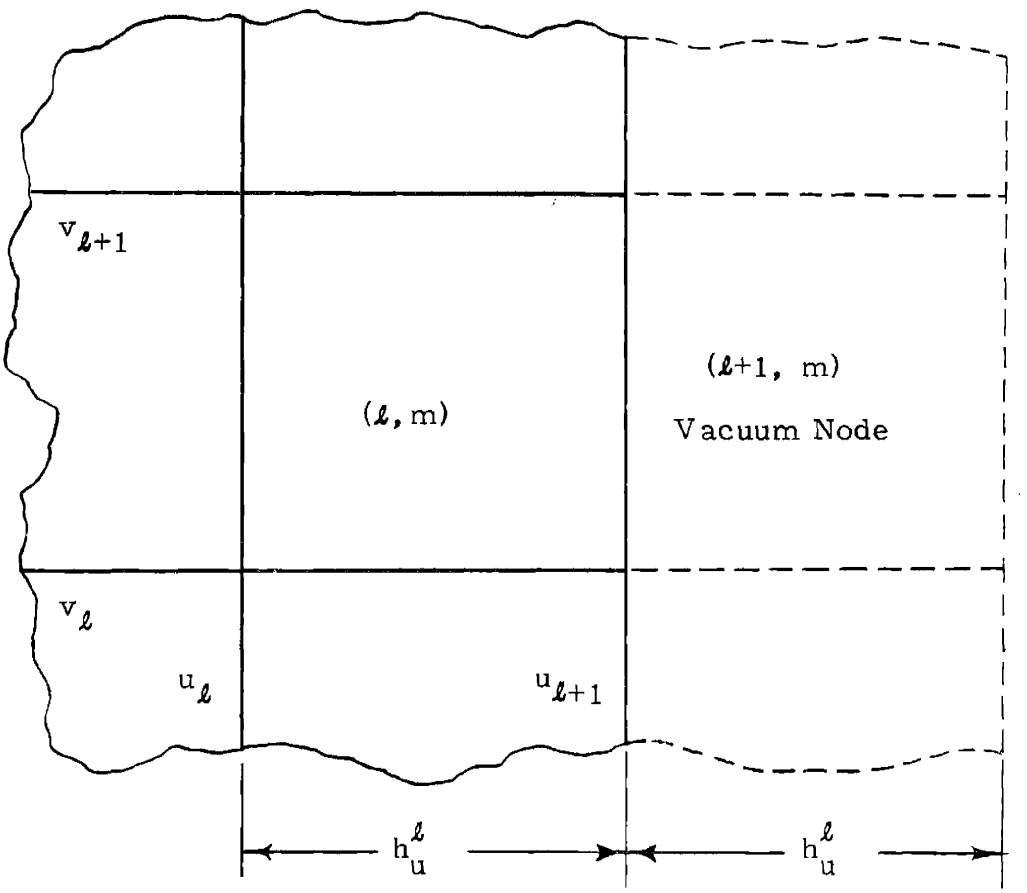

Fig. 1-1 Vacuum Node on Reactor Periphery.

$$J_{g_u}^{(\ell, m)}(u_{\ell+1}) = 0$$

Due to the extensive spatial coupling in the QUANDRY equations, some of the transverse leakage terms are not defined for nodes near the reactor periphery. For example, in Equation (1-23), the term $\bar{S}_{g_u}^{(\ell+1, m)}$ is not defined. To define these terms, QUANDRY introduces imaginary vacuum nodes whose dimensions are identical to those of the adjacent nodes on the reactor periphery. Such a vacuum node is depicted in Fig. 1-1. Since the only function of the average transverse leakage in the vacuum node $\bar{S}_{g_u}^{(\ell+1, m)}$ is to determine the shape of the transverse leakage in the adjacent node, $\bar{S}_{g_u}^{(\ell, m)}(u)$, QUANDRY assumes the average transverse leakage in the vacuum node equals either zero or $-\bar{S}_{g_u}^{(\ell, m)}$. These assumptions are adequate for reactors with water reflectors where the transverse leakage term decreases as one moves outward from reflector to vacuum node.

The actual transverse leakage assumption used in QUANDRY is the programmer's choice. While either assumption results in a shape which tends toward zero as $u \rightarrow u_{\ell+1}$, the assumption that $\bar{S}_{g_u}^{(\ell+1, m)} = -\bar{S}_{g_u}^{(\ell, m)}$ forces $S_{g_u}^{(\ell, m)}(u_{\ell+1})$ closer to zero. In reality, for reactors with water reflectors, the QUANDRY solution is essentially independent of the assumption used for the transverse leakage term in the vacuum node. This is because the transverse leakage term in the reflector is usually relatively small.

1.5 Objectives and Summary

The primary objective of this thesis is to develop an accurate group collapsing procedure for use with the nodal code QUANDRY. Such

a procedure would reduce the required computer memory capacity by a factor of two. Such a procedure would also permit a three or four group problem to be analyzed using a two-group QUANDRY calculation. In Chapter 2, various collapsing procedures will be investigated for one-dimensional reactors. In Chapter 3, collapsing procedures which give promising results in one dimension will be applied in two dimensions. Finally, in Chapter 4, a summary of the results of this thesis will be presented.

CHAPTER 2

GROUP COLLAPSING IN ONE DIMENSION

2.1 Introduction

In Chapter 1, the analytic nodal method QUANDRY was presented. The great advantage of QUANDRY was seen to be that it offered comparable accuracy to finite difference methods while being much more computationally efficient. However, QUANDRY also has some drawbacks. QUANDRY cannot be readily extended beyond two energy groups. Moreover, QUANDRY requires a great deal of computer memory capacity. For large three-dimensional problems, the required memory capacity is excessive. Both these drawbacks could be eliminated by a viable group collapsing procedure.

Chapter 1 also discussed the theoretical basis of the QUANDRY equations. These equations were shown to be formally exact except for the relatively mild approximation that the transverse leakage term in the coupling equations be represented by a quadratic. With the introduction of discontinuity factors, the QUANDRY equations were also shown to be capable of reproducing the exact reactor eigenvalue, node averaged reaction rates and net leakage rates. One of the subtler implications of discontinuity factors is the fact that they allow the exact solution to be reproduced even though the QUANDRY equations are solved in an approximate manner.

In this chapter, various group collapsing procedures are investigated for one-dimensional reactors with both homogeneous and heterogeneous assemblies. All the reactors to be analyzed have water reflectors and two fuel enrichments. Later, a baffle will be introduced. In the analyses of these reactors, both assembly nodes and color set

nodes will be used.

While it is true that one-dimensional reactors are not realistic, analyzing such simple problems often affords valuable insight which would be lost with more complex problems. One-dimensional problems also have the advantage of being relatively inexpensive to run, making it practical to investigate a large number of alternate procedures. Those procedures successfully applied in one dimension can then be tested in two dimensions. Any procedure which is not successful in one dimension is not likely to be successful in two or three dimensions.

2.2 Analysis of a Slab Reactor with Assembly Nodes

Figure 2-1 illustrates a simple one-dimensional reactor with three homogeneous regions. The first and second regions represent homogenized fuel-water mixtures of differing enrichments. The third region is a water reflector. The two-group reference cross sections for each of these regions are listed in Appendix A.

To test the accuracy of various group collapsing procedures, the necessary reference QUANDRY quantities must be determined for comparison purposes. The reference QUANDRY solution was obtained from a two-group QUANDRY calculation, partitioning the reactor so that each node was homogeneous. With the reference two-group solution determined, exact one-group equivalent diffusion theory parameters were obtained by flux weighting:

$$\bar{\Sigma}^{\bar{\Lambda}(\ell)}_{\alpha} \equiv \frac{\Sigma^{(\ell)}_{\alpha_1} \bar{\varphi}^{=(\ell)}_1 + \Sigma^{(\ell)}_{\alpha_2} \bar{\varphi}^{=(\ell)}_2}{\bar{\varphi}^{=(\ell)}_1 + \bar{\varphi}^{=(\ell)}_2} \quad ; \qquad \alpha = f, a \qquad (2\text{-}1)$$

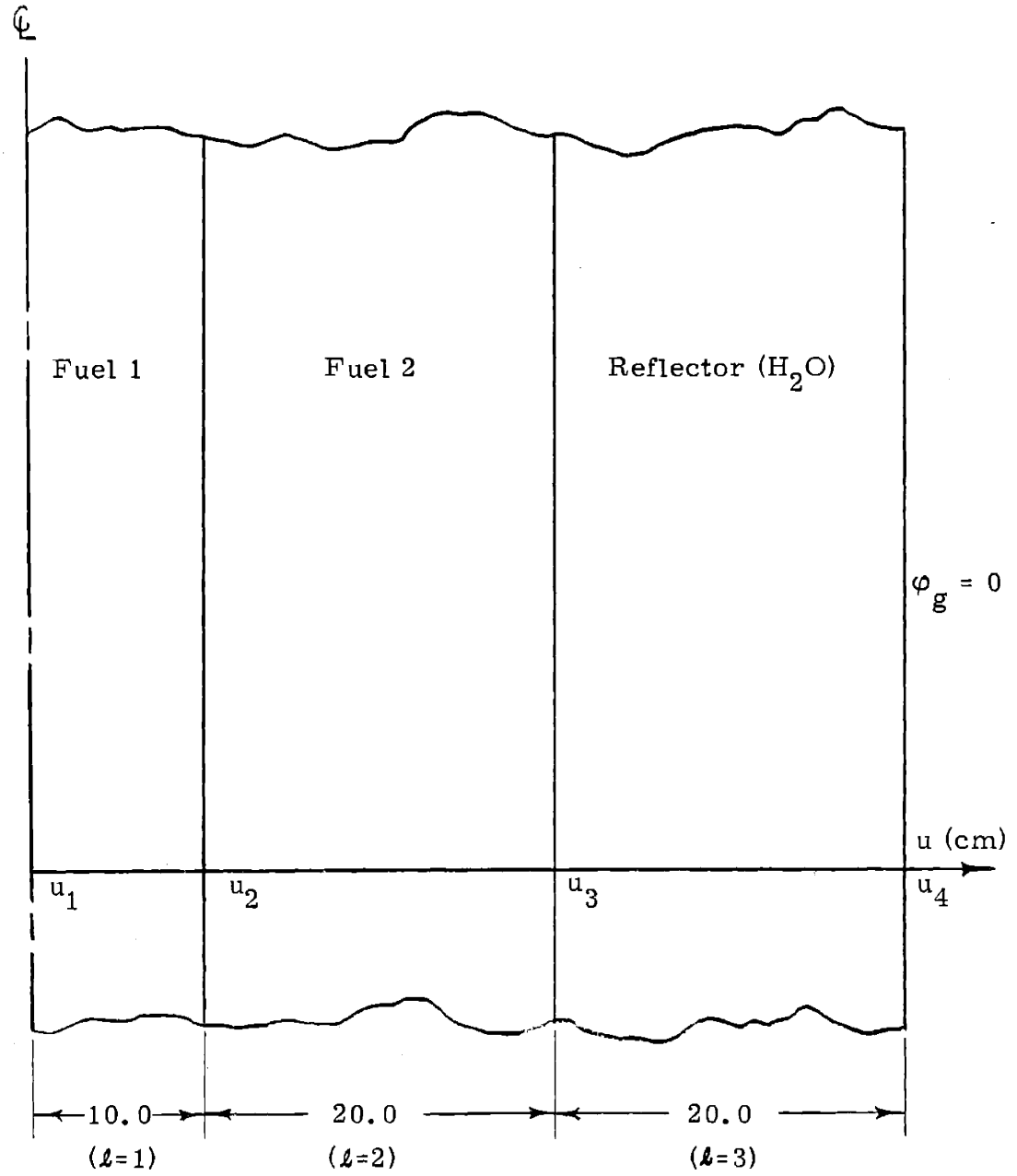

Fig. 2-1 One-Dimensional Three Region Reactor with Assembly Nodes.

$$\bar{\bar{D}}^{(\ell)} \equiv \frac{D_1^{(\ell)} \bar{\bar{\varphi}}_1^{(\ell)} + D_2^{(\ell)} \bar{\bar{\varphi}}_2^{(\ell)}}{\bar{\bar{\varphi}}_1^{(\ell)} + \bar{\bar{\varphi}}_2^{(\ell)}} \tag{2-2}$$

Here

$\bar{\bar{\varphi}}_g^{(\ell)} \equiv$ node averaged, group g flux for node ℓ.

Exact one-group discontinuity factors were obtained by solving the one-group diffusion equation given by Equation (1-14) with the exact one-group equivalent diffusion theory parameters, the exact eigenvalue and the exact net surface currents imposed as boundary conditions. With the resulting homogeneous flux profile, discontinuity factors were calculated from their definitions

$$f_u^{(\ell)}(u_{\ell+1}) \equiv \frac{\bar{\varphi}_{1_u}^{(\ell)}(u_{\ell+1}) + \bar{\varphi}_{2_u}^{(\ell)}(u_{\ell+1})}{\bar{\phi}_u^{(\ell)}(u_{\ell+1})} \tag{2-3}$$

$$f_u^{(\ell)}(u_\ell) \equiv \frac{\bar{\varphi}_{1_u}^{(\ell)}(u_\ell) + \bar{\varphi}_{2_u}^{(\ell)}(u_\ell)}{\bar{\phi}_u^{(\ell)}(u_\ell)} \tag{2-4}$$

where

$\bar{\varphi}_{g_u}^{(\ell)}(u_\ell) \equiv$ exact group g surface flux on u_ℓ face of Node ℓ.

$\bar{\phi}_{g_u}^{(\ell)}(u_\ell) \equiv$ homogeneous group g surface flux on u_ℓ face of Node ℓ.

The exact one-group equivalent diffusion theory parameters and discontinuity factors are listed in Table 2-1. In particular, the small value of $f_u^{(\ell)}(u_{\ell+1})$ for Node 3 should be noted. Since a zero flux

Table 2-1

Exact One-Group Equivalent Diffusion Theory Parameters and Discontinuity Factors for Assembly Nodes.

Node	$\ell = 1$	$\ell = 2$	$\ell = 3$
$\bar{\hat{\Sigma}}_a$ (cm^{-1})	0.02981	0.02685	0.01920
$\nu\bar{\hat{\Sigma}}_f$ (cm^{-1})	0.03001	0.02606	0.0
$\bar{\hat{D}}$ (cm)	1.389	1.368	1.198
$f_u^{(\ell)}(u_\ell)$	0.9980	0.9779	0.8953
$f_u^{(\ell)}(u_{\ell+1})$	1.007	1.145	3.473×10^{-6}

boundary condition was used for this problem, $f_u^{(\ell)}(u_{\ell+1})$ should be zero for Node 3. It was not zero because of machine roundoff error. In any case, the value of $f_u^{(\ell)}(u_{\ell+1})$ for Node 3 is inconsequential; there is no node adjacent to the reflector which requires coupling.

2.2.1 Assembly Calculations

To determine exact one-group equivalent diffusion theory parameters and discontinuity factors, the exact two-group solution had to be known. Of course, if the exact two-group solution is known, there is no point in collapsing and solving the one-group problem. In this section, we hope to obtain accurate one-group quantities by performing a number of "local" assembly calculations.

To isolate these local assembly calculations from the global problem, zero current boundary conditions are imposed on each assembly node. An eigenvalue problem is then solved for each assembly node to obtain the detailed two-group flux distribution and determine approximate one-group equivalent diffusion theory parameters. Discontinuity factors are simply taken to be unity since the assembly nodes for this problem are homogeneous.

While zero current assembly calculations can be applied to nodes with fissionable material present, they cannot be applied to the reflector node. In the reflector, such an approximation would only yield the trivial solution. One way to treat the reflector is to assume that the thermal current is zero on the boundaries of the reflector while the fast current has some nonzero value. The two-group diffusion equations then yield the node averaged fast to slow flux ratio:

$$\frac{\bar{\bar{\varphi}}_1}{\bar{\bar{\varphi}}_2} = \frac{\Sigma_{a_2}}{\Sigma_{21}} \qquad (2\text{-}5)$$

which, when used in Equations (2-1) and (2-2), determines the one-group equivalent diffusion theory parameters for the reflector. Discontinuity factors for the reflector are unity.

Table 2-2 lists the approximate one-group equivalent diffusion theory parameters and discontinuity factors. The accuracy of the zero current assembly calculations used to determine these quantities was assessed by comparing the quantities in Table 2-1 with those in Table 2-2. To facilitate comparisons, an error parameter was defined as

$$\delta\Sigma \equiv \left(\frac{\Sigma_{approx} - \Sigma_{exact}}{\Sigma_{exact}}\right) \qquad (2\text{-}6)$$

The errors in these approximate one-group quantities are listed in Table 2-3.

Examining Table 2-3 shows that the errors in the equivalent diffusion theory parameters and discontinuity factors increase as one moves away from the reactor center. This trend can be explained by examining the exact net current distribution in the reactor depicted in Fig. 2-2. From this figure, it is clear that the zero current approximation used to collapse the equivalent diffusion theory parameters and determine discontinuity factors is less and less accurate as one moves away from the reactor center. The zero current approximation is especially bad at the fuel-reflector interface.

To determine the actual impact of error in the zero current assembly calculations, the global problem was solved using the approximate one-group equivalent diffusion theory parameters and discontinuity factors to obtain the approximate reactor eigenvalue, node averaged reaction rates and net leakage rates. The errors in these approximate

Table 2-2

Approximate One-Group Equivalent Diffusion Theory Parameters and Discontinuity Factors for Assembly Nodes.

Node	$\ell = 1$	$\ell = 2$	$\ell = 3$
$\bar{\Sigma}_a (cm^{-1})$	0.02970	0.02647	0.02118
$\bar{\Sigma}_f (cm^{-1})$	0.02985	0.02559	0.0
$\bar{D}$ (cm)	1.390	1.371	1.144
$f_u^{(\ell)} (u_\ell)$	1.000	1.000	1.000
$f_u^{(\ell)} (u_{\ell+1})$	1.000	1.000	1.000

Table 2-3

Errors in One-Group Equivalent Diffusion Theory Parameters and Discontinuity Factors for Assembly Nodes.

Node	$\ell = 1$	$\ell = 2$	$\ell = 3$
$\delta\bar{\Sigma}_a$ (%)	-0.37	-1.4	+ 10
$\delta\nu\bar{\Sigma}_f$ (%)	-0.53	-1.8	-
$\delta\bar{D}$ (%)	+0.07	+0.19	- 4.5
$\delta f_u^{(\ell)}(u_\ell)$ (%)	+0.20	+2.3	+ 12
$\delta f_u^{(\ell)}(u_{\ell+1})$(%)	-0.69	- 13	-

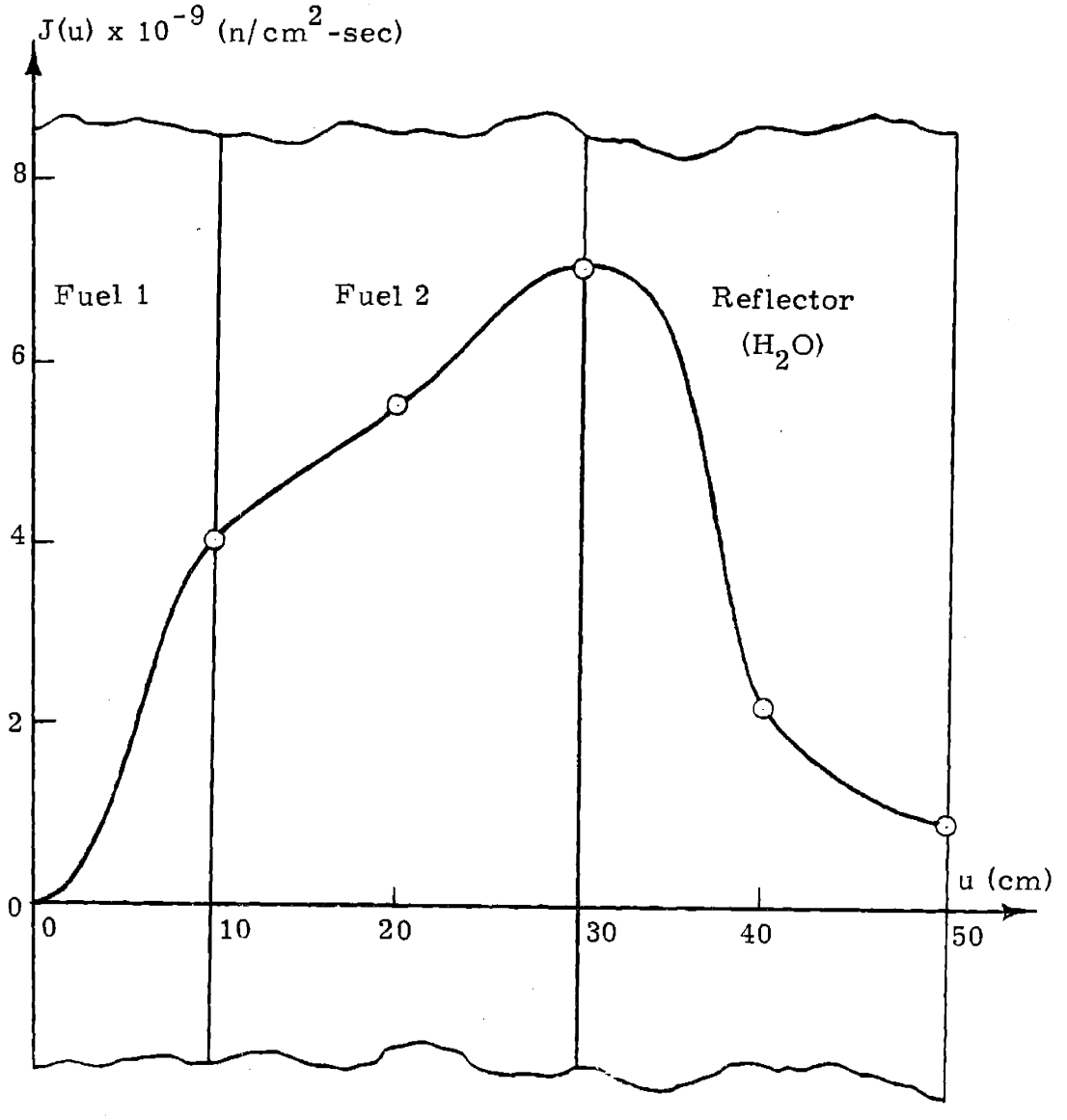

Fig. 2.2 Exact Net Current Distribution.

quantities are listed in Table 2-4.

Examining Table 2-4, we find the reaction rates in Nodes 1 and 2 to be predicted very accurately while the reaction rate in the reflector is poorly predicted. However, knowledge of the reaction rate in the reflector is not crucial.

In contrast to the accurate predictions of nodal reaction rates, errors in the net leakage rates are unacceptably large in all three nodes and especially large for Node 2. These large errors are expected since net leakage rates are sensitive to errors in the discontinuity factors. Finally, reflecting the accuracy of our solution as a whole, the error in the reactor eigenvalue is 0.42%, unacceptably large for such a simple reactor.

2.3 Analysis of a Slab Reactor with Color Set Nodes

The error in one-group equivalent diffusion theory parameters and discontinuity factors obtained from assembly calculations will depend upon the accuracy of the zero current approximation. When adjacent assemblies have similar neutronic characteristics, the zero current approximation will generally yield satisfactory results. However, when adjacent assemblies have drastically different enrichments or when an assembly is adjacent to the reflector, the zero current approximation cannot be expected to yield satisfactory results. In these cases, color set nodes offer a promising alternative to assembly nodes.

The idea behind color sets is to move nodal boundaries to the centers of assemblies where the zero current approximation should be more accurate. The simple three region one-dimensional reactor shown in Fig. 2-1 is depicted in Fig. 2-3 partitioned into color set nodes. One drawback to the use of color sets is that spatial homogenization is

Table 2-4

Errors in One-Group Reactor Eigenvalue, Node Averaged Reaction Rates and Net Leakage Rates for Assembly Nodes.

$\delta k_{eff} = 0.42\%$

Node	$\ell = 1$	$\ell = 2$	$\ell = 3$
$\bar{\hat{\Sigma}}_a \bar{\hat{\phi}}_{Exact}$ (n/cm^3-sec)	3.658×10^9	2.124×10^9	2.859×10^6
$\nu\bar{\hat{\Sigma}}_f \bar{\hat{\phi}}_{Exact}$ (n/cm^3-sec)	3.682×10^9	2.061×10^9	0.0
$\bar{L}_{u_{Exact}}$ (n/cm^2-sec)	3.924×10^9	2.867×10^9	-5.718×10^9
$\bar{\hat{\Sigma}}_a \bar{\hat{\varphi}}_{Approx}$ (n/cm^3-sec)	3.677×10^9	2.124×10^9	2.698×10^9
$\nu\bar{\hat{\Sigma}}_f \varphi_{Approx}$ (n/cm^3-sec)	3.695×10^9	2.053×10^9	0.0
$\bar{L}_{u_{Approx}}$ (n/cm^2-sec)	3.708×10^9	2.501×10^9	-5.396×10^9
$\delta\bar{\hat{\Sigma}}_a \bar{\hat{\phi}}$ (%)	+0.52	+0.05	-5.6
$\delta\nu\bar{\hat{\Sigma}} \bar{\hat{\phi}}$ (%)	+0.35	-0.39	-
$\delta\bar{L}_u$ (%)	-5.5	-13	-5.6

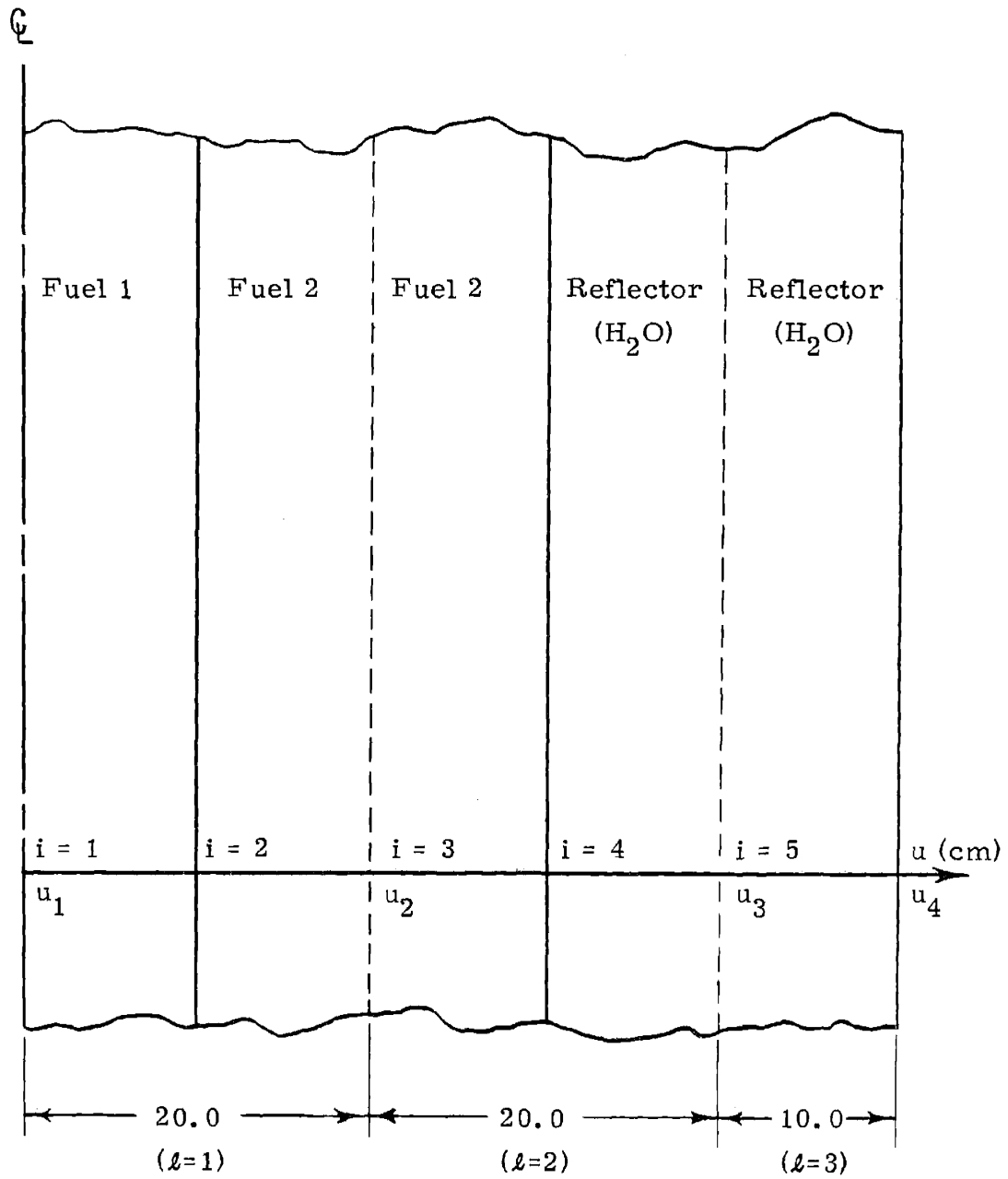

Fig. 2-3 Reactor with Color Set Nodes.

now required for our simple three region reactor. Hopefully, the added error introduced by spatial homogenization will be offset by an improvement in the zero current boundary conditions.

As with assembly nodes, exact one-group equivalent diffusion theory parameters were determined for color set nodes from a two-group fine mesh QUANDRY calculation. The "fineness" of the mesh was such that two-group node averaged fluxes were obtained for each homogeneous region making up the color sets. Since each of the color sets is partitioned into homogeneous regions of equal width:

$$\bar{\hat{\Sigma}}_{\alpha}^{(\ell)} \equiv \frac{\Sigma_{\alpha_1}^{(i)} \bar{\bar{\varphi}}_1^{(i)} + \Sigma_{\alpha_2}^{(i)} \bar{\bar{\varphi}}_2^{(i)} + \Sigma_{\alpha_1}^{(i+1)} \bar{\bar{\varphi}}_1^{(i+1)} + \Sigma_{\alpha_2}^{(i+1)} \bar{\bar{\varphi}}_2^{(i+1)}}{\bar{\bar{\varphi}}_1^{(i)} + \bar{\bar{\varphi}}_2^{(i)} + \bar{\bar{\varphi}}_1^{(i+1)} + \bar{\bar{\varphi}}_2^{(i+1)}} \qquad (2\text{-}7)$$

$$\bar{\hat{D}}^{(\ell)} \equiv \frac{D_1^{(i)} \bar{\bar{\varphi}}_1^{(i)} + D_2^{(i)} \bar{\bar{\varphi}}_2^{(i)} + D_1^{(i+1)} \bar{\bar{\varphi}}_1^{(i+1)} + D_2^{(i+1)} \bar{\bar{\varphi}}_2^{(i+1)}}{\bar{\bar{\varphi}}_1^{(i)} + \bar{\bar{\varphi}}_2^{(i)} + \bar{\bar{\varphi}}_1^{(i+1)} + \bar{\bar{\varphi}}_2^{(i+1)}} \qquad (2\text{-}8)$$

Here, the superscript i denotes the particular homogeneous region. Exact one-group discontinuity factors were determined by solving the one-group neutron diffusion equation for each node using the exact one-group equivalent diffusion theory parameters and the exact net surface currents as boundary conditions. Both the exact one-group equivalent diffusion theory parameters and discontinuity factors are listed in Appendix A.

2.3.1 Color Set Calculations

If we perform zero current color set calculations with QUANDRY, approximate $\bar{\bar{\varphi}}_g^{(i)}$ are obtained which, when substituted into Equations (2-7) and (2-8), determine approximate one-group equivalent diffusion

theory parameters. When used with the zero current boundary conditions and the one-group neutron diffusion equation, these parameters determine approximate one-group discontinuity factors. Approximate one-group equivalent diffusion theory parameters and discontinuity factors are listed in Appendix A.

With color sets, the reflector node was treated differently than with assembly nodes. This was the case because Node 3 is adjacent to a water reflector of substantial width. Thus, the neutron spatial distribution must be very nearly asymptotic and the node averaged fast to slow flux ratio can be obtained by solving the two-group neutron diffusion equations subject to the boundary conditions

$$\varphi_1^{(3)}(u_4) = \varphi_2^{(3)}(u_4) = 0 \qquad (2\text{-}9)$$

$$\frac{\varphi_1^{(3)}(u_3)}{\varphi_2^{(3)}(u_3)} = R \qquad (2\text{-}10)$$

where R is the approximate node averaged fast to slow flux ratio for the adjacent color set node. This approximation turned out to be extremely accurate, predicting the node averaged fast to slow flux ratio for the reflector to within 0.08%. This approximation is not accurate for the assembly node reflector because of the large thermal neutron hump.

The errors in determining the one-group equivalent diffusion theory parameters and discontinuity factors with color set calculations are listed in Table 2-5. Comparing Tables 2-5 and 2-3 makes it apparent that color set calculations are much more accurate for Node 3, less accurate for Node 2 and equally accurate for Node 1. For Node 3, the superiority of the color set approach is expected, given the asymptotic

Table 2-5

Errors in One-Group Equivalent Diffusion Theory Parameters and Discontinuity Factors for Color Set Nodes.

Node	$\ell = 1$	$\ell = 2$	$\ell = 3$
$\delta\bar{\Sigma}_a$ (%)	-0.36	-1.5	-0.05
$\delta\nu\bar{\Sigma}_f$ (%)	-0.47	-11	-
$\delta\bar{D}$ (%)	-0.11	-1.5	-0.09
$\delta f_u^{(\ell)}(u_\ell)$ (%)	-0.29	+27	+85
$\delta f_u^{(\ell)}(u_{\ell+1})$ (%)	+0.19	+0.08	-

neutron distribution. For Node 2, the presence of two drastically different materials greatly increased the sensitivity of the homogenization procedure to errors in the zero current assumption. This increased sensitivity to the "degree of heterogeneity" is starkly exhibited by the 11% error in the fission cross section of Node 2. Finally, equal accuracy is obtained for Node 1 in spite of the fact that Fig. 2-2 shows color sets to have moved the nodal boundary to a location where the zero current approximation is less accurate. Apparently, a fortuitous cancellation of error favored the color set node over the assembly node.

Table 2-6 lists the errors in the reactor eigenvalue, node averaged reaction rates and net leakage rates which result from the use of color set calculations. Comparing the errors here to the errors listed in Table 2-4 for assembly nodes shows that color sets give inferior results for all three nodes. Only the reactor eigenvalue is predicted with equal accuracy. No doubt, the primary reason color sets perform so poorly is the large errors in the one-group quantities of color set Node 2.

2.4 An Iterative Approach

With both assembly nodes and color set nodes, zero current boundary conditions were assumed in order to calculate approximate one-group equivalent diffusion theory parameters and discontinuity factors. While this assumption seemed satisfactory in the reactor interior, it was not satisfactory near the reflector. In this section, we shall attempt to account for the neutron currents near the reflector with an iterative approach.

The idea behind this approach is simple. Namely, the reactor is partitioned into either assembly nodes or color set nodes. Using the zero current approximation to calculate one-group equivalent diffusion

Table 2-6

Errors in One-Group Reactor Eigenvalue, Node Averaged Reaction Rates and Net Leakage Rates for Color Set Nodes.

$\delta k_{eff} = 0.43\%$

Node	$\ell = 1$	$\ell = 2$	$\ell = 3$
$\bar{\Sigma}\bar{\phi}_{Exact}$ (n/cm^3-sec)	3.119×10^9	1.065×10^9	1.176×10^8
$\nu\bar{\Sigma}_f\bar{\phi}_{Exact}$ (n/cm^3-sec)	3.084×10^9	8.189×10^8	0.0
$\bar{L}_{u_{Exact}}$ (n/cm^2-sec)	5.442×10^9	-3.295×10^9	-1.176×10^9
$\bar{\Sigma}_a\bar{\phi}_{Approx}$ (n/cm^3-sec)	3.316×10^9	9.004×10^8	5.894×10^7
$\nu\bar{\Sigma}_f\bar{\phi}_{Approx}$ (n/cm^3-sec)	3.275×10^9	6.272×10^8	0.0
$\bar{L}_{u_{Approx}}$ (n/cm^2-sec)	5.405×10^9	-4.269×10^9	-5.895×10^8
$\delta\bar{\Sigma}_a\bar{\phi}$ (%)	+6.3	-15	-49.9
$\delta\bar{\Sigma}_f\bar{\phi}$ (%)	+6.2	-23	-
$\delta\bar{L}_u$ (%)	-0.68	+30	-49.9

theory parameters and discontinuity factors, the global reactor problem is solved. From this global solution, net surface currents and surface fluxes are used to perform improved assembly calculations or color set calculations. The resulting equivalent diffusion theory parameters and discontinuity factors are used, in turn, to obtain an improved one-group solution. This global-local iteration cycle is then repeated until a satisfactory solution is obtained.

To proceed, consider the two-group diffusion equations for an arbitrary homogeneous node:

$$-D_1 \frac{d^2}{du^2} \varphi_1(u) + (\Sigma_{R_1} - \frac{1}{\lambda}\nu\Sigma_{f_1})\varphi_1(u) - \frac{1}{\lambda}\nu\Sigma_{r_2}\varphi_2(u) = 0 \tag{2-11}$$

$$-D_2 \frac{d^2}{du^2} \varphi_2(u) + \Sigma_{a_2}\varphi_2(u) - \Sigma_{21}\varphi_1(u) = 0 \tag{2-12}$$

These two equations have the general solutions[9]

$$\varphi_1(u) = C_1 \frac{s}{\mu} \sin \mu u + C_2 s \cos \mu u + C_3 t \sinh \nu u + C_4 t \cosh \nu u \tag{2-13}$$

$$\varphi_2(u) = C_1 \frac{1}{\mu} \sin \mu u + C_2 \cos \mu u + C_3 \sinh \nu u + C_4 t \cosh \nu u \tag{2-14}$$

where

$$\mu^2 = -\frac{1}{2}\left(\frac{\Sigma_{a_2}}{D_2} + \frac{\Sigma_{R_1} - \frac{1}{\lambda}\nu\Sigma_{f_1}}{D_1}\right) + \left[\left(\frac{\Sigma_{a_2}}{2D_2} - \frac{\Sigma_{R_1} - \frac{1}{\lambda}\nu\Sigma_{f_1}}{2D_1}\right)^2 + \frac{\frac{1}{\lambda}\nu\Sigma_{f_2}\Sigma_{21}}{D_1 D_2}\right]^{\frac{1}{2}} \tag{2-15}$$

$$\nu^2 = \frac{1}{2}\left(\frac{\Sigma_{a_2}}{D_2} + \frac{\Sigma_{R_1} - \frac{1}{\lambda}\nu\Sigma_{f_1}}{D_1}\right) + \left[\left(\frac{\Sigma_{a_2}}{2D_2} - \frac{\Sigma_{R_1} - \frac{1}{\lambda}\nu\Sigma_{f_1}}{2D_1}\right)^2 + \frac{\frac{1}{\lambda}\nu\Sigma_{f_2}\,\Sigma_{21}}{D_1 D_2}\right]^{\frac{1}{2}} \tag{2-16}$$

$$s = \frac{D_2\mu^2 + \Sigma_{a_2}}{\Sigma_{21}} \tag{2-17}$$

$$t = \frac{-D_2\nu^2 + \Sigma_{a_2}}{\Sigma_{21}} \tag{2-18}$$

If the four constants C_1, C_2, C_3 and C_4 could be determined from the approximate one-group global solution, improved one-group equivalent diffusion theory parameters and discontinuity factors could be readily calculated.

In fact, the constants C_1, C_2, C_3 and C_4 can be determined given the net surface currents and surface fluxes from the one-group global solution. If we add Equations (2-13) and (2-14), an analytic expression for the one-group flux is obtained:

$$\varphi(u) = \varphi_1(u) + \varphi_2(u) \tag{2-19}$$

Similarly, an analytic expression for the one-group net current is

$$J(u) = J_1(u) + J_2(u) \tag{2-20}$$

where

$$J_1(u) = -D_1 \frac{d}{du}\varphi_1(u) \tag{2-21}$$

$$J_2(u) = - D_2 \frac{d}{du} \varphi_2(u) \qquad (2\text{-}22)$$

Now, Equations (2-19) and (2-20) must equal the net surface currents and surface fluxes obtained from the one-group global solutions. Thus, a set of four equations and four unknowns results which allows the constants C_1, C_2, C_3 and C_4 to be determined. In matrix form, these equations are

$$\begin{vmatrix} \varphi(u_\ell) \\ \varphi(u_{\ell+1}) \\ J(u_\ell) \\ J(u_{\ell+1}) \end{vmatrix} = \begin{vmatrix} 0 & 1+s \\ \frac{(1+s)}{\mu} \sin(\mu u_{\ell+1}) & (1+s)\cos(\mu u_{\ell+1}) \\ D_1 s + D_2 & 0 \\ -(s D_1 + D_2)\cos(\mu u_{\ell+1}) & \mu(D_1 s + D_2)\sin(\mu u_{\ell+1}) \end{vmatrix}$$

$$\begin{vmatrix} 0 & 1+t & & C_1 \\ (1+t)\sinh(\nu u_{\ell+1}) & (1+t)\cosh(\nu u_{\ell+1}) & & C_2 \\ -\nu(D_1 t + D_2) & 0 & & C_3 \\ -\nu(D_1 t + D_2)\cosh)(\nu u_{\ell+1}) & \nu(D_1 t + D_2)\sinh(\nu u_{\ell+1}) & & C_4 \end{vmatrix} \qquad (2\text{-}23)$$

$$\{\Phi\} \equiv [A]\{C\} \qquad (2\text{-}24)$$

$$\{C\} = [A]^{-1}\{\varphi\} \qquad (2\text{-}25)$$

The above approach can also be extended to heterogeneous nodes. For color set nodes constructed with only two homogeneous regions, an

analytic approach remains practical. However, since four new constants are added with each additional homogeneous region introduced into the color set, the size of the matrices quickly gets out of hand. For example, a one-dimensional PWR assembly has upwards of seventeen homogeneous regions, requiring the inversion of a 68 x 68 matrix with no simple structure. Clearly, an iterative approach involving such a difficult calculation will not be practical. To handle color sets with many homogeneous regions, numerical techniques are much more tractable. Regardless of the degree of heterogeneity present, there is no reason why this approach should not converge to the exact solution.

Unfortunately, this iterative approach is not practical in two dimensions, the main reason being that two-dimensional problems must be solved numerically and, for a 17 x 17 node, the problem is just too big. A secondary drawback is that the one-group global solution only yields surface averaged net currents and surface averaged fluxes. No information is given concerning the shape of the fluxes and net currents on nodal surfaces. Such information would be necessary for convergence to the exact solution. While ways exist to approximate the shapes of the net surface currents and surface fluxes, this particular iterative approach was not investigated further.[5]

An alternate approach which should be practical in two dimensions, though the shapes of the net surface currents and the surface fluxes must still be approximated, uses the surface averaged fast to slow flux ratios from adjacent assemblies or color sets to "split" the one-group surface fluxes from the global solution. These surface averaged fast to slow flux ratios are obtained from assembly calculations or color set calculations. The split two-group surface fluxes then serve as boundary

conditions to calculate improved one-group equivalent diffusion theory parameters and discontinuity factors. Presumably, repeating this cycle will result in a still more accurate solution. However, unlike the previous iterative approach, this approach will not converge to the exact solution since there is no way to update the surface averaged fast to slow flux ratios.

2.4.1 Updated Assembly Calculations

To perform updated assembly calculations with fluxes imposed as boundary conditions, the mesh centered finite difference code CITATION was used.[6] The details of CITATION will not be discussed in this thesis. QUANDRY was not used to perform updated assembly calculations because, at the time of this investigation, it was not capable of solving fixed source problems.

Table 2-7 lists the errors in the updated one-group equivalent diffusion theory parameters and discontinuity factors for assembly nodes. The actual values for these updated quantities are listed in Appendix B. Comparing these errors to the errors in Table 2-3 makes it apparent that our iterative approach markedly improves these one-group quantities for all three nodes.

Table 2-8 compares the reactor eigenvalue, node averaged reaction rates and net leakage rates of the exact one-group solution with the approximate one-group solution obtained using both updated equivalent diffusion theory parameters and updated discontinuity factors. Comparing Tables 2-4 and 2-8 makes it apparent that updating these one-group quantities results in a much more satisfactory solution, particularly when the reactor eigenvalue and nodal leakage rates are of concern.

Table 2-7

Errors in One-Group Equivalent Diffusion Theory Parameters and Discontinuity Factors for Assembly Nodes After One Iteration

Node	$\ell = 1$	$\ell = 2$	$\ell = 3$
$\delta\bar{\Sigma}_a$ (%)	-0.03	-0.93	-2.1
$\delta\nu\bar{\Sigma}_f$ (%)	-0.03	-1.0	-
$\delta\bar{D}$ (%)	-0.07	-0.15	-1.1
$\delta f_u^{(\ell)}(u_\ell)$ (%)	-0.20	-0.34	2.8
$\delta f_u^{(\ell)}(u_{\ell+1})$ (%)	+0.20	+6.3	-

Table 2-8

Errors in One-Group Reactor Eigenvalue, Node Averaged Reaction Rates, and Net Leakage Rates for Assembly Nodes After Updating Both Equivalent Diffusion Theory Parameters and Discontinuity Factors

δk_{eff} = 0.06%

Node	ℓ = 1	ℓ = 2	ℓ = 3
$\bar{\Sigma}_a \bar{\phi}_{Exact}$ (n/cm^3-sec)	3.658 x 10^9	2.124 x 10^9	2.859 x 10^8
$\nu\bar{\Sigma}_f \bar{\phi}_{Exact}$ (n/cm^3-sec)	3.682 x 10^9	2.061 x 10^9	0.0
$\bar{L}_{u_{Exact}}$ (n/cm^2-sec)	3.924 x 10^9	2.867 x 10^9	-5.718 x 10^9
$\bar{\Sigma}_a \bar{\phi}_{Approx}$ (n/cm^3-sec)	3.677 x 10^9	2.115 x 10^9	2.803 x 10^8
$\nu\bar{\Sigma}_f \bar{\phi}_{Approx}$ (n/cm^3-sec)	3.702 x 10^9	2.051 x 10^9	0.0
$\bar{L}_{u_{Approx}}$ (n/cm^2-sec)	3.914 x 10^9	2.794 x 10^9	-5.605 x 10^9
$\delta\bar{\Sigma}_a \bar{\phi}$ (%)	+0.52	-0.42	-2.0
$\delta\nu\bar{\Sigma}_f \bar{\phi}$ (%)	+0.54	-0.49	-
$\delta\bar{L}_u$ (%)	-0.25	-2.6	-2.0

Finally, we found that failing to update both equivalent diffusion theory parameters and discontinuity factors together can actually result in a solution which is less accurate than a solution obtained using zero current assembly calculations. This fact implies that it is better to use relatively inaccurate discontinuity factors which reflect errors in the one-group equivalent diffusion theory parameters rather than use relatively accurate discontinuity factors which do not reflect errors in the one-group equivalent diffusion theory parameters.

2.4.2 Updated Color Set Calculations

Table 2-9 lists the errors in the updated equivalent diffusion theory parameters and discontinuity factors for color set nodes. The actual values for these updated quantities are listed in Appendix B. Comparing Tables 2-5 and 2-9 shows that the updated one-group equivalent diffusion theory parameters were markedly improved for all three nodes. Improvement was especially dramatic for Node 2. However, when the updated discontinuity factors are compared to their zero current counterparts, no improvement is apparent.

Table 2-10 compares the reactor eigenvalue, node averaged reaction rates and net leakage rates of the exact one-group solution with the approximate one-group solution obtained using both updated equivalent diffusion theory parameters and updated discontinuity factors. Comparing Tables 2-6 and 2-10 shows that the iterative approach is less accurate than the solution obtained with zero current color set calculations.

Why is the iterative approach less successful with color set nodes than with assembly nodes? The underlying reason is that with color sets an additional error is introduced through the spatial homogenization

Table 2-9

Errors in One-Group Equivalent Diffusion Theory Parameters and Discontinuity Factors for Color Set Nodes After One Iteration

Node	$\ell = 1$	$\ell = 2$	$\ell = 3$
$\delta\bar{\Sigma}_a$ (%)	-0.35	+0.16	-0.04
$\delta\nu\bar{\Sigma}_f$ (%)	-0.29	+0.83	-
$\delta\bar{D}$ (%)	-0.14	+0.21	+0.03
$\delta f_u^{(\ell)}(u_\ell)$ (%)	-0.69	+25	+81
$\delta f_u^{(\ell)}(u_{\ell+1})$ (%)	+2.7	+27	-

Table 2-10

Errors in One-Group Reactor Eigenvalue, Node Averaged Reaction Rates and Net Leakage Rates for Color Set Nodes After Updating Both Equivalent Diffusion Theory Parameters and Discontinuity Factors

$\delta k_{eff} = 1.38\%$

Node	$\ell = 1$	$\ell = 2$	$\ell = 3$
$\bar{\Sigma}_a \bar{\phi}_{Exact}$ (n/cm^3-sec)	3.119×10^9	1.065×10^9	1.176×10^8
$\nu\bar{\Sigma}_f \bar{\phi}_{Exact}$ (n/cm^3-sec)	3.084×10^9	8.189×10^8	0.0
$\bar{L}_{u_{Exact}}$ (n/cm^2-sec)	5.442×10^9	-3.295×10^9	-1.176×10^9
$\bar{\Sigma}_a \bar{\phi}_{Approx}$ (n/cm^3-sec)	3.184×10^9	9.705×10^8	8.459×10^7
$\nu\bar{\Sigma}_f \bar{\phi}_{Approx}$ (n/cm^3-sec)	3.150×10^9	7.509×10^8	0.0
$\bar{L}_{u_{Approx}}$ (n/cm^2-sec)	4.662×10^9	-3.117×10^9	-8.460×10^8
$\delta\bar{\Sigma}_a \bar{\phi}$ (%)	+2.1	-8.9	-28
$\delta\nu\bar{\Sigma}_f \bar{\phi}$ (%)	+2.1	-8.3	-
$\delta\bar{L}_u$ (%)	-14	-5.4	-28

procedure. Also, for this particular reactor, color sets move the nodal boundaries to locations where the zero current approximation is somewhat less accurate than with assembly nodes. The poor values obtained for the one-group equivalent diffusion theory parameters lead, in turn, to a poor solution to the global problem. Thus, when the one-group surface fluxes were split, new color set calculations were performed with poor boundary conditions.

In Tables 2-11 through 2-14, errors in determining the surface averaged fast to slow flux ratios and the one-group surface fluxes are listed for both assembly nodes and color set nodes. These tables show that color sets approximate the surface averaged fast to slow flux ratios much more accurately than do assembly nodes, while assembly nodes approximate the one-group surface fluxes much more accurately than do color set nodes. After one iteration, the overall error in splitting the one-group surface fluxes is given in Tables 2-15 and 2-16.

We conclude that our iterative approach appears to be capable of providing accurate results. Unfortunately, the amount of work required to obtain an adequate solution to realistic problems seems to be prohibitive. For a one-dimensional reaction with heterogeneous nodes, the results of our updated color set calculations indicate that at least two iterations will be required. For two-dimensional heterogeneous nodes, an even greater number of iterations may be necessary. Thus, the iterative approach was abandoned.

2.5 Albedo Boundary Conditions

The stumbling block for each of the previous collapsing methods has been their inability to determine accurate one-group equivalent diffusion theory parameters and discontinuity factors for nodes adjacent

Table 2-11

Error in Approximating Surface Averaged Fast to Slow Flux Ratios for Assembly Nodes

Surface	u_1	u_2	u_3	u_4
$(\bar{\varphi}_1/\bar{\varphi}_2)_{Exact}$	9.037	8.274	3.522	1.250
$(\bar{\varphi}_1/\bar{\varphi}_2)_{Approx}$	9.000	8.250	4.464	1.429
$\delta(\bar{\varphi}_1/\bar{\varphi}_2)$ (%)	-0.41	-0.29	+27	+14

Table 2-12

Error in Approximating Surface Averaged Fast to Slow Flux Ratios for Color Set Nodes

Surface	u_1	u_2	u_3	u_4
$(\bar{\varphi}_1/\bar{\varphi}_2)_{Exact}$	9.037	7.519	1.305	1.250
$(\bar{\varphi}_1/\bar{\varphi}_2)_{Approx}$	9.009	7.560	1.304	1.267
$\delta(\bar{\varphi}_1/\bar{\varphi}_2)$ (%)	-0.31	+0.54	-0.08	+1.4

Table 2-13

Error in One-Group Surface Fluxes Obtained from Approximate One-Group Solution with Assembly Nodes

Surface	u_1	u_2	u_3	u_4
$\bar{\varphi}_{Exact}$	1.273×10^{11}	1.140×10^{11}	3.958×10^{10}	0.00
$\bar{\varphi}_{Approx}$	1.284×10^{11}	1.148×10^{11}	3.954×10^{10}	0.00
$\delta\bar{\varphi}$ (%)	+0.86	+0.70	-0.10	-

Table 2-14

Error in One-Group Surface Fluxes Obtained from Approximate One-Group Solution with Color Set Nodes

Surface	u_1	u_2	u_3	u_4
$\bar{\varphi}_{Exact}$	1.269×10^{11}	8.033×10^{10}	1.203×10^{10}	0.00
$\bar{\varphi}_{Approx}$	1.338×10^{11}	8.941×10^{10}	1.173×10^{10}	0.00
$\delta\bar{\varphi}$ (%)	+5.4	+11	-2.5	-

Table 2-15

Error in Splitting Surface Flux
for Assembly Nodes

Surface	u_1	u_2	u_3	u_4
$\bar{\varphi}_{1_{Exact}}$	1.145×10^{11}	1.017×10^{11}	3.087×10^{10}	0.00
$\bar{\varphi}_{2_{Exact}}$	1.267×10^{10}	1.228×10^{10}	8.766×10^{9}	0.00
$\bar{\varphi}_{1_{Approx}}$	1.156×10^{11}	1.024×10^{11}	3.230×10^{10}	0.00
$\bar{\varphi}_{2_{Approx}}$	1.284×10^{10}	1.241×10^{10}	7.236×10^{9}	0.00
$\delta\bar{\varphi}_1$ (%)	+0.96	+0.69	+4.6	-
$\delta\bar{\varphi}_2$ (%)	-1.3	+1.1	-17	-

Table 2-16

Error in Splitting Surface Flux for Color Set Nodes

Surface	u_1	u_2	u_3	u_4
$\bar{\varphi}_{1_{Exact}}$	1.145×10^{11}	7.108×10^{10}	6.831×10^{9}	0.00
$\bar{\varphi}_{2_{Exact}}$	1.267×10^{10}	9.454×10^{10}	5.235×10^{9}	0.00
$\bar{\varphi}_{1_{Approx}}$	1.204×10^{11}	7.896×10^{10}	6.639×10^{9}	0.00
$\bar{\varphi}_{2_{Approx}}$	1.337×10^{10}	1.045×10^{10}	5.091×10^{9}	0.00
$\delta\bar{\varphi}_1$ (%)	+5.2	+11	-2.8	-
$\delta\bar{\varphi}_2$ (%)	+5.5	+10	-2.8	-

to the reflector. This stumbling block should be removed if the exact albedo boundary conditions are used for collapsing calculations on the reactor periphery. Of course, exact albedo boundary conditions can only be determined from the exact solution. Thus, the practical application of such a collapsing procedure will ultimately depend upon the ability to approximate accurate albedos with local calculations. Currently, researchers at MIT are investigating methods which will approximate albedo boundary conditions. This thesis will proceed on the assumption that these investigations will be successful.

2.5.1 Assembly Nodes with Albedo Boundary Conditions

Consider the reactor depicted in Fig. 2-1. An assembly calculation was performed for Node 2 using exact two-group albedos for the right hand boundary conditions and the zero current assumption for the left hand boundary conditions. Table 2-17 lists the errors in the one-group equivalent diffusion theory parameters and discontinuity factors for both Nodes 1 and 2. Here, Node 1 was collapsed with the usual zero current assembly calculation. Comparing Tables 2-3 and 2-17 makes it apparent that the albedo assembly calculation is much more accurate than the zero current assembly calculation.

Solving the one-group problem using the approximate equivalent diffusion theory parameters and discontinuity factors gives excellent results as shown by Table 2-18.

2.5.2 Color Set Nodes with Albedo Boundary Conditions

Consider the reactor depicted in Fig. 2-3. A color set calculation was performed for Node 2 using the exact two-group albedos for the right hand boundary conditions and the zero current assumption for the left hand boundary conditions. Table 2-19 lists the errors in the one-group

Table 2-17

Errors in One-Group Equivalent Diffusion Theory Parameters and Discontinuity Factors for Assembly Nodes with Albedo Boundary Conditions

Node	$\ell = 1$	$\ell = 2$
$\delta\bar{\Sigma}_a$ (%)	-0.37	+0.48
$\delta\nu\bar{\Sigma}_f$ (%)	-0.53	+0.61
$\delta\bar{D}$ (%)	+0.07	-0.07
$\delta f_u^{(\ell)}(u_\ell)$ (%)	+0.20	+1.0
$\delta f_u^{(\ell)}(u_{\ell+1})$ (%)	-0.69	-0.04

Table 2-18

Errors in One-Group Reactor Eigenvalue, Node Averaged Reaction Rates and Net Leakage Rates for Assembly Nodes with Albedo Boundary Conditions

$\delta k_{eff} = -0.02\%$

Node	$\ell = 1$	$\ell = 2$
$\overline{\hat{\Sigma}}_a \overline{\hat{\phi}}_{Exact}$ (n/cm^3-sec)	3.658×10^9	2.124×10^9
$\nu\overline{\hat{\Sigma}}\overline{\hat{\phi}}_{Exact}$ (n/cm^3-sec)	3.682×10^9	2.061×10^9
$\overline{L}_{u_{Exact}}$ (n/cm^2-sec)	3.924×10^9	2.867×10^9
$\overline{\hat{\Sigma}}_a \overline{\hat{\phi}}_{Approx}$ (n/cm^3-sec)	3.650×10^9	2.127×10^9
$\nu\overline{\hat{\Sigma}}_f \overline{\hat{\phi}}_{Approx}$ (n/cm^3-sec)	3.668×10^9	2.068×10^9
$\overline{L}_{u_{Approx}}$ (n/cm^2-sec)	3.858×10^9	2.943×10^9
$\delta\overline{\hat{\Sigma}}_a \overline{\hat{\phi}}$ (%)	-0.22	+0.14
$\delta\nu\overline{\hat{\Sigma}}_f \overline{\hat{\phi}}$ (%)	-0.38	+0.34
$\delta\overline{L}_u$ (%)	-1.7	+2.6

Table 2-19

Errors in One-Group Equivalent Diffusion Theory Parameters and Discontinuity Factors for Color Set Nodes with Albedo Boundary Conditions

Node	$\ell = 1$	$\ell = 2$
$\delta\bar{\Sigma}_a$ (%)	-0.36	-0.52
$\delta\nu\bar{\Sigma}_f$ (%)	-0.47	-4.6
$\delta\bar{D}$ (%)	-0.11	-0.72
$\delta f_u^{(\ell)}(u_\ell)$ (%)	-0.29	-19
$\delta f_u^{(\ell)}(u_{\ell+1})$ (%)	+0.19	+22

equivalent diffusion theory parameters and discontinuity factors for Nodes 1 and 2. Here, Node 1 was collapsed with the usual zero current color set calculation. The actual values of the approximate one-group quantities for Node 2 are listed in Appendix C. Comparing Tables 2-5 and 2-19 shows that albedo boundary conditions improve the equivalent diffusion theory parameters by a factor of two. However, discontinuity factors are not improved at all.

Table 2-20 lists the errors in reactor eigenvalue, node averaged reaction rates and net leakage rates for the one-group solution obtained using the approximate equivalent diffusion theory parameters and discontinuity factors. Comparing Tables 2-18 and 2-20 shows that albedo boundary conditions give much less accurate results with color set nodes than with assembly nodes. As before, the culprit is Node 2, where the presence of two materials having drastically different neutronic characteristics makes the spatial homogenization process very sensitive to any errors in the boundary conditions.

2.6 Analysis of a One-Dimensional Reactor with Heterogeneous Assemblies

In the previous section, we found that the use of albedo boundary conditions gave excellent results with assembly nodes and relatively poor results with color set nodes. Therefore, color set nodes will be abandoned at this point in favor of assembly nodes. The use of albedo boundary conditions will be investigated further with heterogeneous assemblies.

A one-dimensional reactor with heterogeneous assemblies, a baffle, reflector and two fuel enrichments is depicted in Fig. 2-4. Exact one-group equivalent diffusion theory parameters and discontinuity factors

Table 2-20

Errors in One-Group Reactor Eigenvalue, Node Averaged Reaction Rates and Net Leakage Rates for Color Set Nodes with Albedo Boundary Conditions

$\delta k_{eff} = -0.59\%$

Node	$\ell = 1$	$\ell = 2$
$\overline{\hat{\Sigma}}_a \overline{\hat{\phi}}_{Exact}$ (n/cm^3-sec)	3.119×10^9	1.065×10^9
$\nu\overline{\hat{\Sigma}}_f \overline{\hat{\phi}}_{Exact}$ (n/cm^3-sec)	3.084×10^9	8.189×10^8
$\overline{L}_{u_{Exact}}$ (n/cm^2-sec)	5.442×10^9	-3.295×10^9
$\overline{\hat{\Sigma}}_a \overline{\hat{\phi}}_{Approx}$ (n/cm^3-sec)	3.268×10^9	9.294×10^8
$\nu\overline{\hat{\Sigma}}_f \overline{\hat{\phi}}_{Approx}$ (n/cm^3-sec)	3.231×10^9	6.851×10^8
$\overline{L}_{u_{Approx}}$ (n/cm^2-sec)	5.194×10^9	-3.607×10^9
$\delta\overline{\hat{\Sigma}}_a \overline{\hat{\phi}}$ (%)	+4.8	-13
$\delta\nu\overline{\hat{\Sigma}}_f \overline{\hat{\phi}}$ (%)	+4.8	-16
$\delta\overline{L}_u$ (%)	-4.6	+9.5

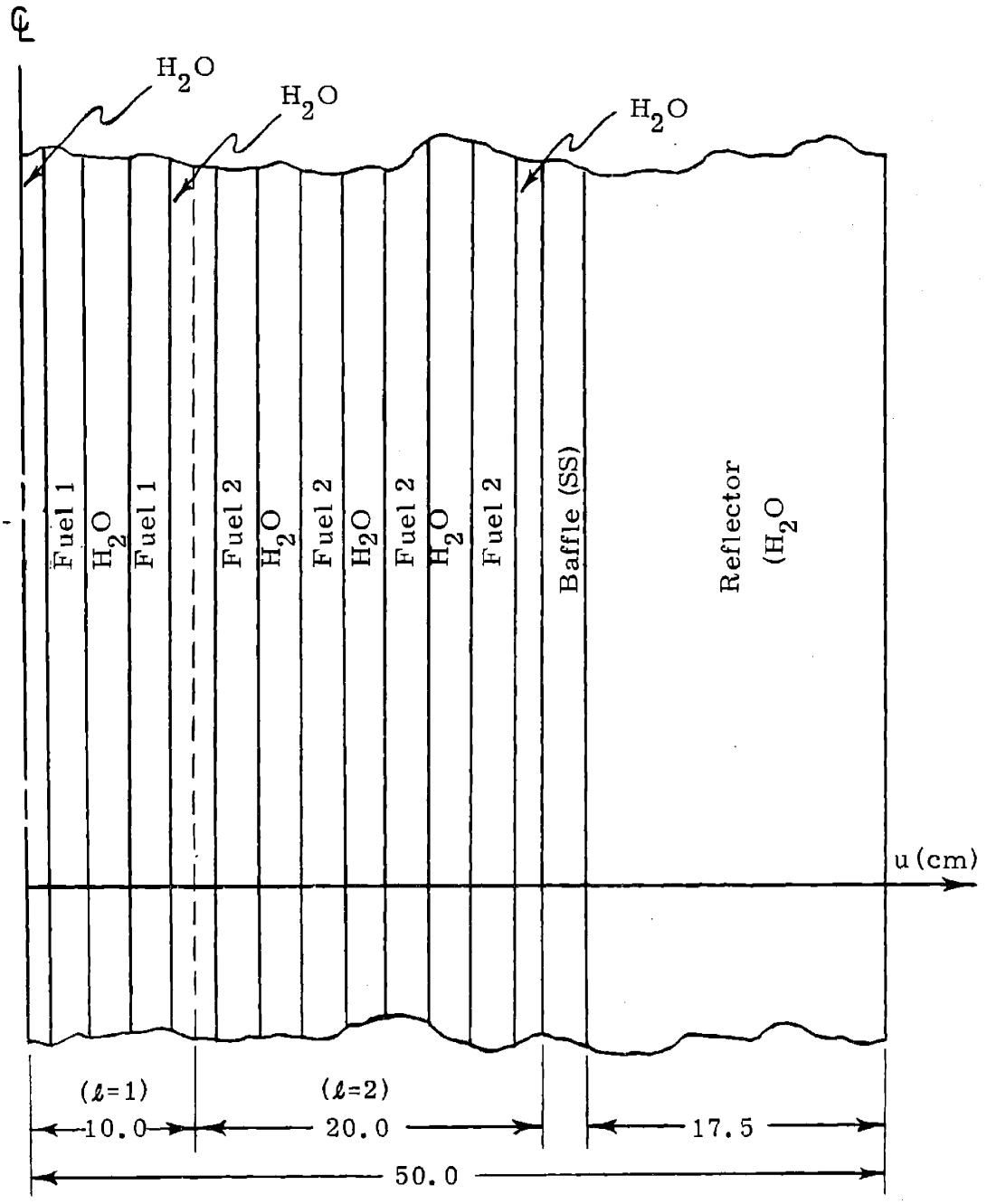

Fig. 2-4 One-Dimensional Reactor with Heterogeneous Assembly Nodes.

were determined for this reactor from a fine mesh QUANDRY calculation. These exact quantities are listed in Appendix C.

Approximate one-group equivalent diffusion theory parameters and discontinuity factors were obtained in the usual manner. In the reactor interior, a zero current assembly calculation was performed. Adjacent to the baffle, the exact two-group albedo boundary conditions were imposed on the right side of the assembly and zero current boundary conditions were imposed on the left side of the assembly. Table 2-21 lists the errors in these approximate quantities. As expected, agreement with the exact quantities is excellent. In part, this excellent agreement is due to the symmetric nature of the heterogeneous assemblies and the fact that the nodal boundary is located at the center of a homogeneous region where the zero current approximation should be relatively accurate.

In Table 2-22, the approximate reactor eigenvalue, node averaged reaction rates and net leakage rates are compared with the exact values. Agreement is excellent, though not quite so good as when homogeneous assembly nodes were analyzed with albedo boundary conditions. Of course, the solution with homogeneous assemblies should be better than with heterogeneous assemblies since there is additional error introduced by spatial homogenization. It should be noted that the size of the error in the net leakage rate for Node 2 is deceptively large; the errors in the individual net surface currents are

$$\delta J_u^{(2)}(u_2) = -0.39\%$$

$$\delta J_u^{(2)}(u_3) = -1.8\%$$

Table 2-21

Errors in One-Group Equivalent Diffusion Theory Parameters and Discontinuity Factors for Heterogeneous Assembly Nodes with Albedo Boundary Conditions

Nodes	$\ell = 1$	$\ell = 2$
$\delta \overline{\overline{\Sigma}}_a$ (%)	+0.07	-0.28
$\delta \overline{\overline{\nu\Sigma}}_f$ (%)	+0.02	-0.30
$\delta \overline{\overline{D}}$ (%)	+0.03	+0.04
$\delta f_u^{(\ell)}(u_\ell)$ (%)	-0.13	+0.87
$\delta f_u^{(\ell)}(u_{\ell+1})$ (%)	+1.2	-1.8

Table 2-22

Errors in One-Group Reactor Eigenvalue, Node Averaged Reaction Rates and Net Leakage Rates for Heterogeneous Assembly Nodes with Albedo Boundary Conditions

$\delta k_{eff} = 0.13\%$

Node	$\ell = 1$	$\ell = 2$
$\overline{\hat{\Sigma}}_a \overline{\hat{\phi}}$ Exact (n/cm^3-sec)	4.407×10^9	2.474×10^9
$\nu\overline{\hat{\Sigma}}_f \overline{\hat{\phi}}$ Exact (n/cm^3-sec)	3.893×10^9	1.955×10^9
$\overline{L}_{u\,Exact}$ (n/cm^2-sec)	6.169×10^9	9.899×10^8
$\overline{\hat{\Sigma}}_a \overline{\hat{\phi}}$ Approx (n/cm^3-sec)	4.457×10^9	2.448×10^9
$\nu\overline{\hat{\Sigma}}_f \overline{\hat{\phi}}$ Approx (n/cm^3-sec)	3.935×10^9	1.934×10^9
$\overline{L}_{u\,Approx}$ (n/cm^2-sec)	6.145×10^9	8.899×10^8
$\delta\overline{\hat{\Sigma}}_a \overline{\hat{\phi}}$ (%)	+1.1	-1.0
$\delta\nu\overline{\hat{\Sigma}}_f \overline{\hat{\phi}}$ (%)	+1.1	-1.1
$\delta\overline{L}_u$ (%)	-0.39	-10

2.7 Summary

In this chapter, various methods were investigated whereby a problem which would nominally be solved using two groups was solved using one group. In the interest of minimizing computational cost and gaining physical insight, simple one-dimensional reactors were analyzed using both assembly nodes and color set nodes. At first, the investigation was limited to a reactor with homogeneous assemblies. Later, heterogeneous assemblies were introduced.

The first method investigated determined one-group equivalent diffusion theory parameters and discontinuity factors from assembly calculations using the zero current approximation. While this method approximated the node averaged reaction rates to within 1% in the two fuel regions, the net leakage rates and the reactor eigenvalue were not determined with satisfactory accuracy.

In an attempt to mitigate the effect of the reflector on the adjacent node, color sets were introduced. Unfortunately, color sets gave less satisfactory results than assembly nodes. There were two reasons for the poor performance of color sets. First, one of the color set nodes was composed of two materials with drastically different neutronic characteristics, thereby increasing the sensitivity of the spatial homogenization procedure to errors in the zero current approximation. Second, for this particular reactor, color sets actually moved the nodal boundaries to locations where the zero current approximation was less accurate.

Another method investigated in this chapter involved iterating between assembly calculations and the one-group global solution. Specifically, approximate one-group equivalent diffusion theory

parameters and discontinuity factors were obtained from zero current assembly calculations. Solving the one-group problem with these approximate quantities yielded approximate one-group net surface currents and surface fluxes for each node. The one-group surface fluxes were then split into two groups using an approximate fast to slow flux ratio. The approximate fast to slow flux ratios were obtained by taking the average of the fast to slow flux ratios on adjacent nodal surfaces. These surface fast to slow flux ratios were obtained from the zero current assembly calculations. Finally, with two-group surface fluxes known for each node, improved assembly calculations were performed.

This iterative approach was applied to color set nodes as well as assembly nodes. For assembly nodes, only one iteration was required to reduce the error in net leakage rates for the fuel nodes to less than 3% and the error in the reactor eigenvalue to less than 0.1%. The errors in the node averaged reaction rates for the fuel regions were less than 1%. For color set nodes, one iteration was not sufficient. The poor performance with color sets was due to the inaccuracy of the zero current color set calculations. While a second iteration would probably yield satisfactory results, this fact was not confirmed; we felt that an approach which required more than one iteration would be prohibitively cumbersome.

The last method investigated in this chapter attempted to circumvent the problems inherent with the reflector by replacing the reflector with albedo boundary conditions. Albedo boundary conditions were used with both assembly nodes and color set nodes. For assembly nodes, results were excellent. Node averaged reaction rates had errors less

than 1%, while net leakage rates had errors less than 3%. The reactor eigenvalue had an error of less than 0.02%. For color sets, results were poor. The poor performance of color sets was due to the inaccuracy of the zero current approximation for the nodal boundary in the reactor interior.

Of all the methods investigated in this chapter, the use of albedo boundary conditions with assembly nodes was the most promising. Extending this method to a one-dimensional reactor with heterogeneous assemblies and a baffle gave excellent results. Node averaged reaction rates had errors less than 1%, while net surface currents had errors less than 2%. The reactor eigenvalue had an error less than 0.1%.

CHAPTER 3

GROUP COLLAPSING IN TWO DIMENSIONS

3.1 Introduction

In Chapter 2, various group collapsing procedures were investigated. The zero current approximation was found to be satisfactory in the reactor interior, but it was inadequate near the reflector. In an attempt to account for the neutron currents near the reflector, an iterative approach was developed. While this approach gave accurate results, it was abandoned as computationally inefficient. Finally, we found that the effect of the reflector could be satisfactorily accounted for by collapsing assembly nodes adjacent to the reflector with the proper albedo boundary conditions. Of course, the usefulness of such a procedure will ultimately depend upon the ability to determine accurate albedo boundary conditions without solving the global problem.

In this chapter, the use of assembly calculations with albedo boundary conditions is extended to two dimensions. Two reactors will be analyzed, EPRI-9 and CISE, each representing a different reactor type. EPRI-9 models a simplified PWR core. CISE models a simplified BWR core.

3.2 Analysis of EPRI-9

Figure 3-1 illustrates the EPRI-9 reactor core. EPRI-9 includes a baffle, reflector and two fuel enrichments. The two-group reference cross sections for these materials are listed in Appendix D. The heterogeneous nature of EPRI-9 is shown by the assembly in Fig. 3-2. All assemblies in EPRI-9 have identical geometries, differing only in fuel enrichment. Each assembly has seventeen water holes placed

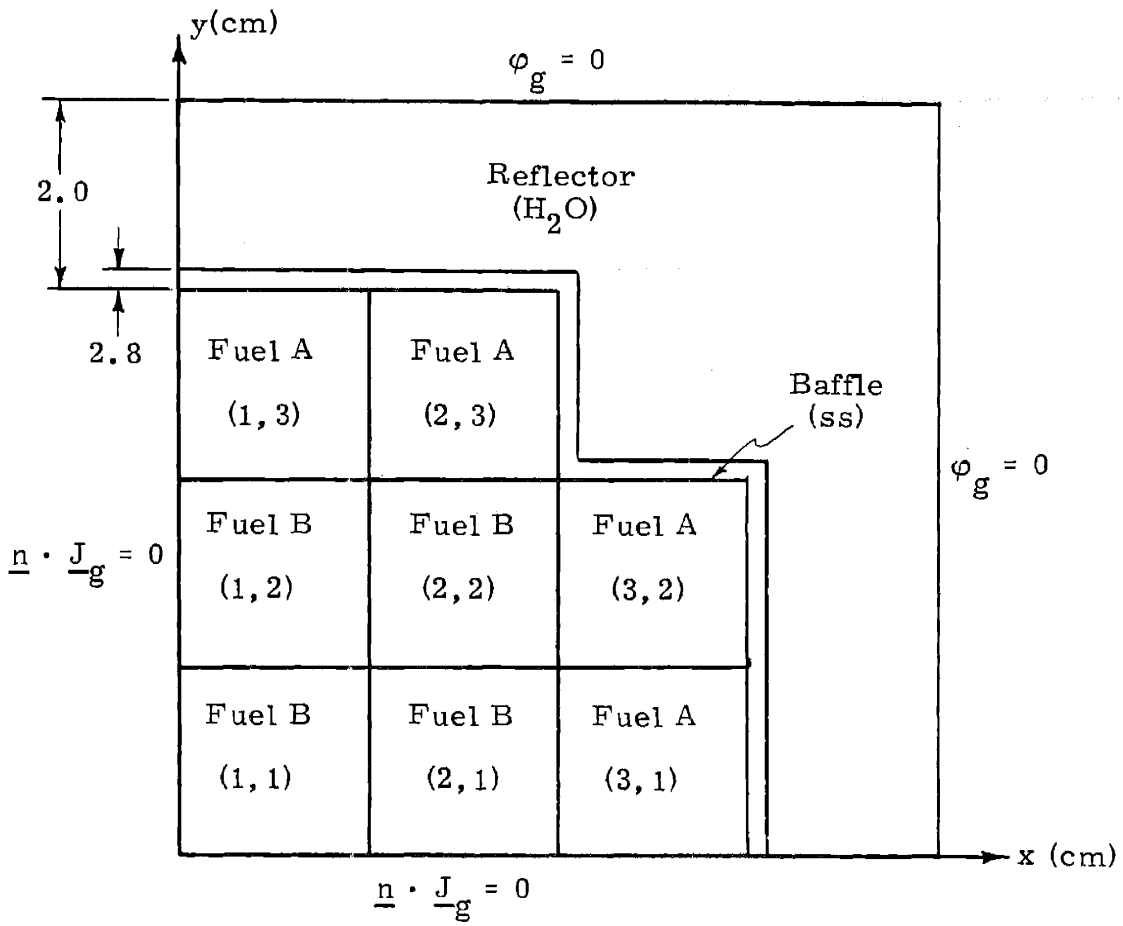

Fig. 3-1 EPRI-9 Reactor (Heterogeneous Nature of Nodes Not Shown Here).

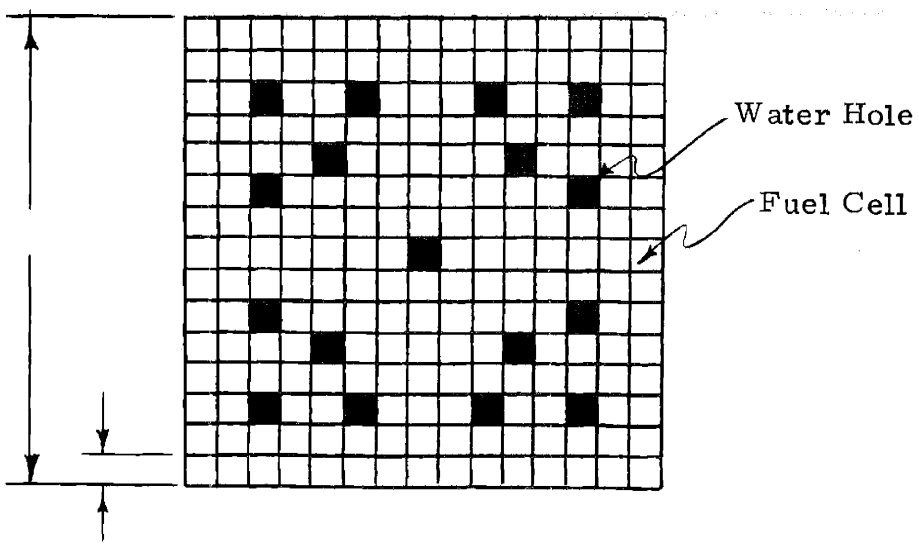

Fig. 3-2 EPRI-9 Assembly.

symmetrically about a 15 x 15 mesh. Each mesh represents a homogenized fuel cell.

To obtain the exact two-group solution to EPRI-9, a fine mesh QUANDRY calculation was performed. Exact one-group equivalent diffusion theory parameters and discontinuity factors were then determined using the exact heterogeneous flux distribution and the exact net surface currents. Exact albedo boundary conditions were determined from their definitions:

$$\bar{\alpha}_g^{(\ell,m)}(u_\ell) \equiv \frac{\int_{v_m}^{v_{m+1}} \varphi_g^{(\ell,m)}(u_\ell, v)\, dv}{\int_{v_m}^{v_{m+1}} J_g^{(\ell,m)}(u_\ell, v)\, dv}$$

$$= \frac{\bar{\varphi}_g^{(\ell,m)}(u_\ell)}{\bar{J}_g^{(\ell,m)}(u_\ell)} ; \quad g = 1, 2 \qquad (3\text{-}1$$

where Node (ℓ, m) is a large, assembly-sized node. These exact quantities are all listed in Appendix D.

To determine approximate equivalent diffusion theory parameters and discontinuity factors, the usual zero current assembly calculations were performed in the reactor interior. For assemblies adjacent to the baffle, in contrast to our experience with one-dimensional problems, it was necessary to assume a shape for the albedos before assembly calculations could be performed. For CISE, as well as EPRI-9, the shape was assumed to be flat.

Altogether, four assembly calculations were required. These

assemblies are identified in Fig. 3-1 as Nodes (1,2), (1,3), (2,3) and (2,2). Table 3-1 lists the errors in the approximate one-group equivalent diffusion theory parameters and discontinuity factors for each of the above assemblies. The actual values of these approximate quantities are given in Appendix D.

When we examine Table 3-1, it is apparent that the errors in Node (2,3) are relatively large when compared to the errors in the other nodes, though the magnitudes of these errors are still quite acceptable on an absolute scale. The relatively large errors in Node (2,3) can be attributed to the fact that the albedo shape is not at all flat for nodes situated at the corner of the reactor. Figures 3-3 and 3-4 illustrate the actual albedo shapes determined from the fine mesh QUANDRY calculation.[7] While these figures show the assumption of a flat albedo to be a poor approximation for Node (2,3), they show this to be an excellent assumption for Node (1,3).

Table 3-2 lists the errors in the reactor eigenvalue, node averaged reaction rates and net leakage rates of the approximate one-group solution determined using exact albedo boundary conditions. Agreement with the exact solution is excellent; the reactor eigenvalue is predicted to within 0.03%, the maximum error in node averaged reaction rates is 0.99%, and the maximum error in net leakage rates is 5.8%.

To gauge the amount of error introduced via the collapsing process versus error introduced through the spatial homogenization process, EPRI-9 was also analyzed with two groups, making the same approximations as in the one-group case. Namely, for assemblies in the reactor interior, two-group equivalent diffusion theory parameters and discontinuity factors were determined from zero current assembly calculations.

Table 3-1

Errors in One-Group Equivalent Diffusion Theory Parameters and Discontinuity Factors for EPRI-9 Assembly Nodes

Node (i, j)	(1, 2)	(1, 3)	(2, 3)	(2, 2)
$\delta\bar{\Sigma}_a$ (%)	0.73	-0.64	-0.38	-0.49
$\delta\nu\bar{\Sigma}_f$ (%)	0.95	-0.91	-0.48	-0.71
$\delta\bar{D}$ (%)	-0.17	+0.07	+0.07	+0.03
$\delta f_x^{(i,j)}(x_i)$ (%)	-0.24	-0.18	+2.8	-0.93
$\delta f_x^{(i,j)}(x_{i+1})$ (%)	0.95	+0.23	-5.3	0.32
$\delta f_y^{(i,j)}(y_j)$ (%)	-0.40	-0.79	+1.9	0.93
$\delta f_y^{(i,j)}(y_{j+1})$ (%)	1.2	+0.04	-5.5	0.32

Table 3-2

Errors in One-Group Reactor Eigenvalue, Node Averaged Reaction Rates and Net Leakage Rates for EPRI-9

δk_{eff} = 0.03%

(1, 3) +0.59 +0.32 -3.2	(2, 3) +0.45 +0.35 -1.6	
(1, 2) -0.10 +0.12 +5.8	(2, 2) -0.22 +0.01 -2.7	
(1, 1) -0.95 -0.99 -1.0		Node (i, j) $\delta\bar{\Sigma}_a\bar{\phi}$ (%) $\delta\nu\bar{\Sigma}_f\bar{\phi}$ (%) $\delta(\bar{L}_x+\bar{L}_y)$ (%)

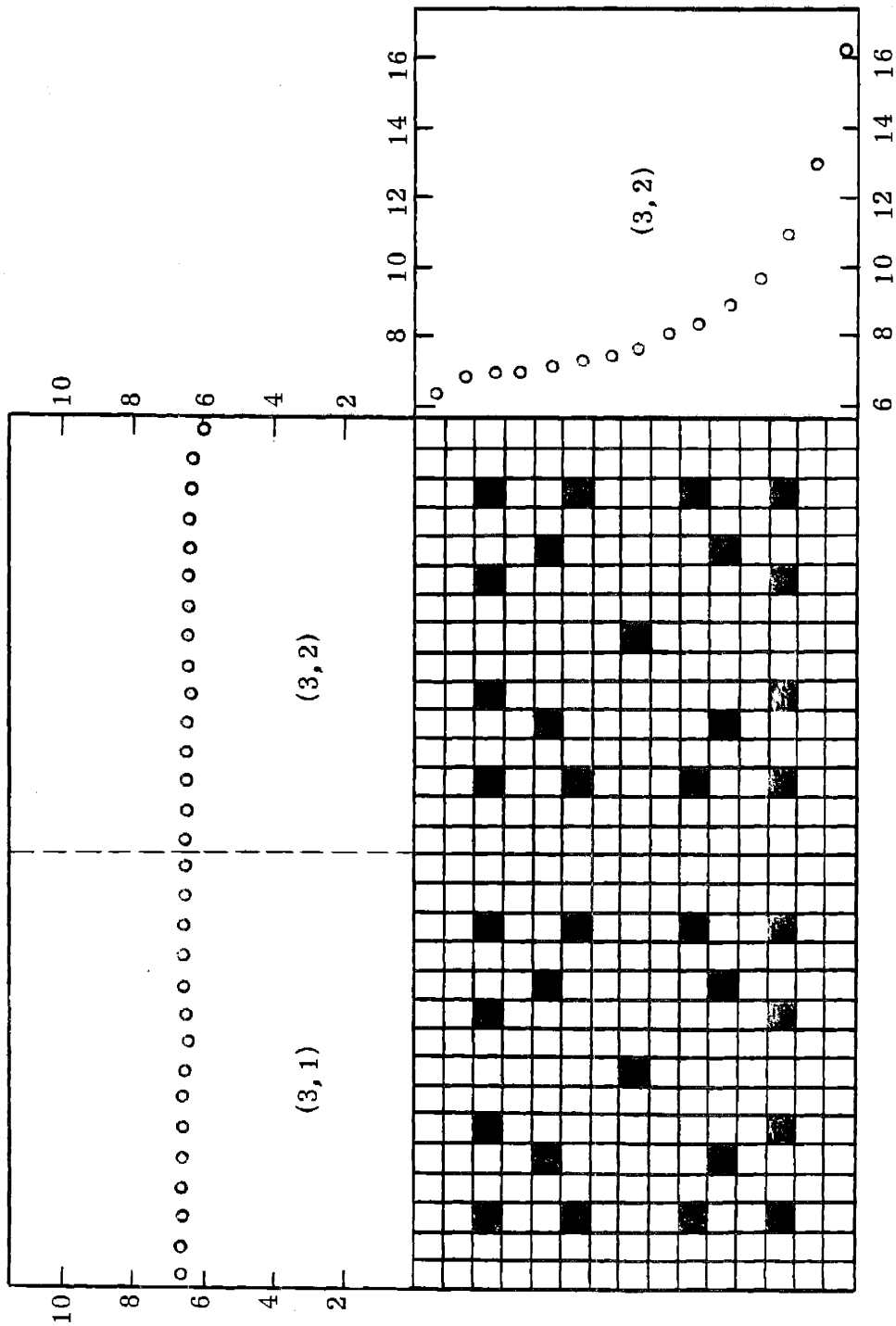

Fig. 3-3 Fast Group Albedo Shape.

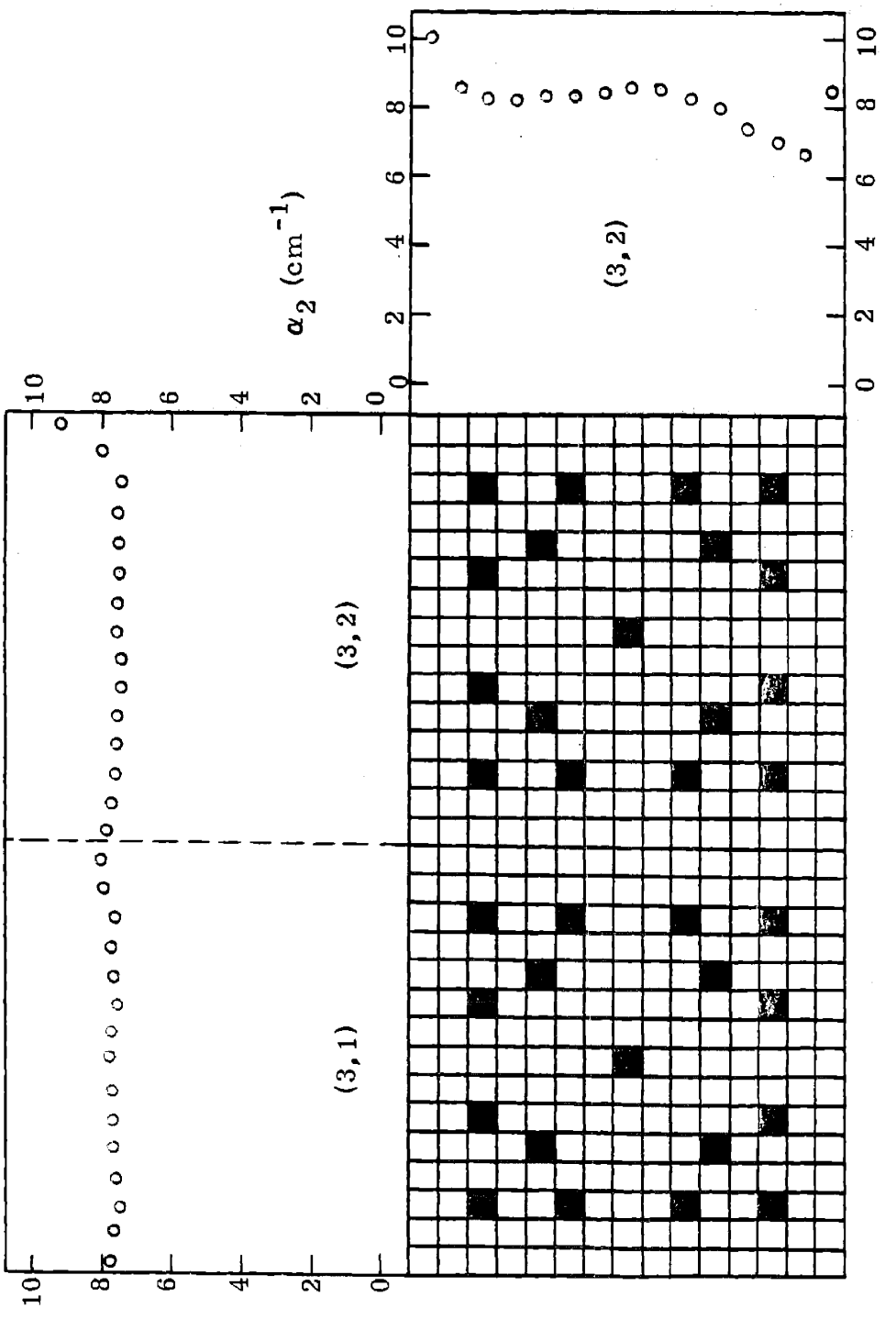

Fig. 3-4 Thermal Group Albedo Shapes.

Adjacent to the baffle,the appropriate two-group albedo boundary conditions were used for assembly calculations. Table 3-3 lists the errors in the reactor eigenvalue, node averaged reaction rates and net leakage rates for this approximate two-group solution.

Comparing Tables 3-2 and 3-3 makes it apparent that one-group gives better estimates of the reactor eigenvalue and node averaged reaction rates, while two-groups gives better estimates of net leakage rates. Thus, the collapsing process actually seems to compensate for some of the errors introduced by spatial homogenization. Why is this the case? Because of the relatively small differences between the one- and two-group solutions for EPRI-9, this question will not be addressed here, but will instead be addressed in some detail after we have presented results for the CISE case.

3.2.1 Approximate Albedo Boundary Conditions

Of course, the accuracy of a procedure which collapses two-groups to one-group using approximate albedo boundary conditions will depend, to a large degree, on the accuracy with which approximate albedo boundary conditions can be determined. While this thesis will not discuss the accuracies inherent in the various schemes used to obtain approximate albedo boundary conditions, an attempt will be made to determine the "sensitivity" of the one-group solution to errors in approximate albedo boundary conditions. Clearly, a one-group solution which is extremely sensitive to such errors must be looked upon with suspicion.

To test the sensitivity of the EPRI-9 problem, a one-group solution was obtained using approximate albedo boundary conditions determined by solving the two-group problem with quarter assembly nodes.[8] Zero

Table 3-3

Errors in Two-Group Reactor Eigenvalue, Node Averaged Reaction Rates and Net Leakage Rates for EPRI-9

$\delta k_{eff} = 0.12\%$

(1,3) +1.15 +1.18 +0.01	(2,3) +0.82 +0.91 +0.28	
(1,2) -0.65 -0.63 -3.6	(2,2) +0.11 +0.09 -1.4	
(1,1) -1.14 -1.20 -4.3		Node (i,j) $\delta\bar{\Sigma}_a\bar{\phi}$ (%) $\delta\nu\bar{\Sigma}_f\bar{\phi}$ (%) $\delta(\bar{L}_x+\bar{L}_y)$ (%)

current color set calculations were used to determine the two-group equivalent diffusion theory parameters and discontinuity factors for these quarter assembly nodes. The errors in the reactor eigenvalue, node averaged reaction rates and net leakage rates for this approximate one-group solution are listed in Table 3-4. Tables 3-5 and 3-6 list the errors in the approximate albedo boundary conditions. The magnitude of error in these approximate albedo boundary conditions is not at all insignificant.

A comparison of Tables 3-2 and 3-6 shows that the use of approximate albedo boundary conditions has a minimal effect on the one-group EPRI-9 solution. Thus, it seems safe to conclude that for this type of reactor, the one-group solution is relatively insensitive to errors in approximate albedo boundary conditions. While it may be that reactors containing control rods or burnable poison rods will be more sensitive to errors in approximate albedo boundary conditions, this thesis will not pursue the matter further.

3.3 Analysis of CISE

The CISE reactor is illustrated in Fig. 3-5. CISE includes a reflector, but no baffle, cruciform control rods and two fuel enrichments. The two-group reference cross sections for these materials are listed in Appendix E. The heterogeneous nature of CISE is shown by the assembly in Fig. 3-6. Region I represents a homogenized fuel-water mixture. For those assemblies with control rods, Region II represents control rod material and Region III represents water. For those assemblies without control rods, both Regions II and III represent water. All the assemblies in CISE have identical geometries.

Table 3-4

Errors in One-Group Reactor Eigenvalue, Node Averaged Reaction Rates and Net Leakage Rates for EPRI-9 with Approximate Albedos

$\delta k_{eff} = -0.04\%$

(1, 3) -0.08 -0.35 -3.0	(2, 3) -0.96 -1.15 -3.2	
(1, 2) +0.49 +0.72 +9.0	(2, 2) +0.32 +0.11 -1.6	
(1, 1) +0.10 +0.10 +2.4		Node (i, j) $\delta \bar{\hat{\Sigma}}_a \bar{\hat{\varphi}}$ (%) $\delta \nu \bar{\hat{\Sigma}}_f \bar{\hat{\varphi}}$ (%) $\delta (\bar{L}_x + \bar{L}_y)$ (%)

Table 3-5

Errors in Approximate Two-Group Albedo Boundary Conditions for EPRI-9

Node (i, j)	Direction u	Group g	$(\bar{\alpha}_g^{(\ell, m)}(u_{\ell+1}))_{Exact}$ (cm^{-1})	$(\bar{\alpha}_g^{(\ell, m)}(u_{\ell+1}))_{Approx}$ (cm^{-1})	$\delta(\bar{\alpha}_g^{(\ell, m)}(u_{\ell+1}))$ %
(1, 3)	Y	1	6.464	6.181	-4.4
	Y	2	7.763	7.192	-7.4
(2, 3)	X	1	9.031	8.938	-1.0
	X	2	11.110	7.882	-29
	Y	1	6.333	6.086	-3.9
	Y	2	7.649	7.186	-6.0

Table 3-6

Errors in Approximate One-Group Albedo Boundary Conditions for EPRI-9

Node (i, j)	Direction u	Group g	$(\bar{\alpha}_g^{(\ell, m)}(u_{\ell+1}))_{Exact}$ (cm^{-1})	$(\bar{\alpha}_g^{(\ell, m)}(u_{\ell+1}))_{Approx}$ (cm^{-1})	$\delta(\bar{\alpha}_g^{(\ell, m)}(u_{\ell+1}))$ %
(1, 3)	Y	1	6.566	6.253	-4.8
(2, 3)	X	1	9.189	8.841	-3.8
	Y	1	6.436	6.181	-4.0

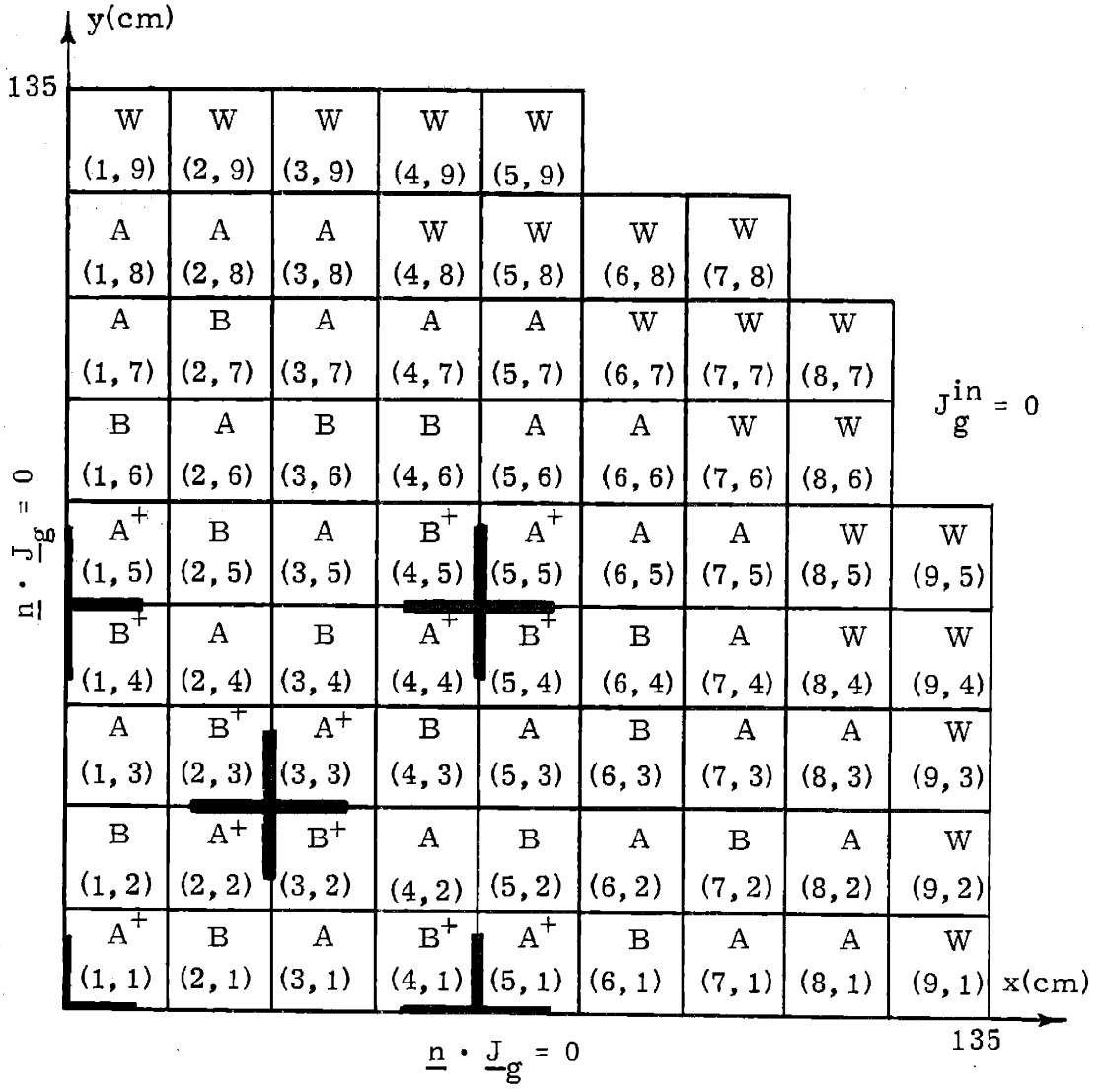

W = water

A = high enrichment

A^+ = high enrichment with control rod

B = low enrichment

B^+ = low enrichment with control rod

Fig. 3-5 CISE Reactor (Heterogeneous Nature of Nodes Not Shown Here).

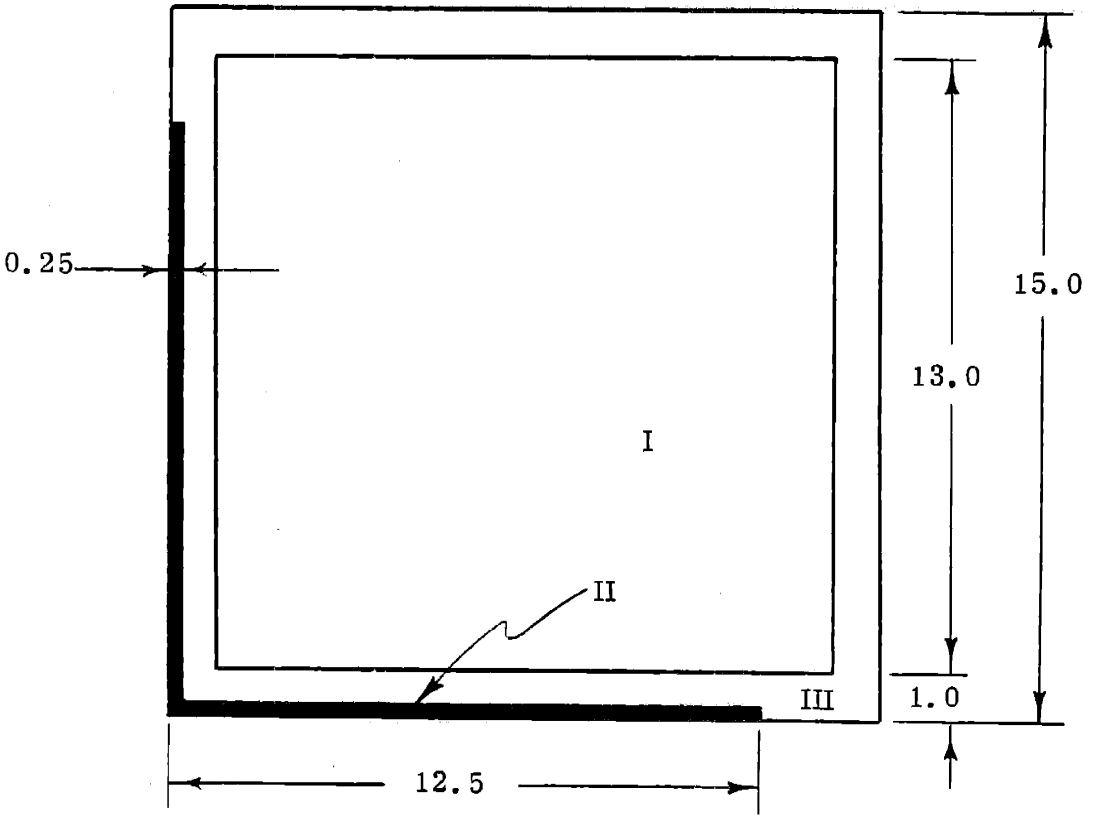

Fig. 3-6 CISE Assembly.

To obtain the exact two-group solution to CISE, a fine mesh QUANDRY calculation was performed. Exact albedo boundary conditions were obtained from this solution and are listed in Appendix E. Exact one-group equivalent diffusion theory parameters and discontinuity factors were not calculated for CISE; the fine mesh QUANDRY calculation was run a number of years ago and the necessary information was not available.

In the interior of CISE, approximate equivalent diffusion theory parameters and discontinuity factors were determined from the usual zero current assembly calculations. A total of four zero current assembly calculations were performed, one for each unique assembly type. These four assembly types are identified in Fig. 3-5 as Nodes (1,5), (2,5), (1,4) and (2,4). For assemblies adjacent to the reflector, assembly calculations were performed with the appropriate albedo boundary conditions. Altogether, five of these assembly calculations were required. The assemblies used for these calculations are identified in Fig. 3-5 as Nodes (1,8), (3,8), (4,7), (5,7) and (6,6). An assembly calculation was not performed for Node (2,8) since the albedo boundary conditions for this node were nearly identical to those for Node (1,8).

Table 3-7 lists the errors in the reactor eigenvalue, relative nodal power fractions and net leakage rates of the approximate one-group solution determined using exact albedo boundary conditions. Agreement with the exact solution is excellent; the reactor eigenvalue is predicted to within 0.02%, the maximum error in the relative nodal power fraction is 2.8%, and the maximum error in net leakage rate is 18.11%. Both the exact one-group solution and the approximate one-group solution are

Table 3-7

Errors in One-Group Reactor Eigenvalue, Relative Nodal Power Fractions and Net Leakage Rates for CISE

$\delta k_{eff} = -0.02\%$

+0.15 -0.34	+0.03 -0.46	+0.59 +0.34				
+0.75 +1.6	+0.36 +1.7	+0.66 +1.2	-0.69 =0.92	-0.53 -0.80		
+0.56 +2.6	+0.78 +1.6	+0.45 +1.8	+0.41 +2.2	+0.38 +0.97	-0.82 -0.70	δP (%) $\delta(\overline{L}_x + \overline{L}_y)$(%)
-2.8 +14.	+0.82 +2.1	+1.4 +2.3	-3.0 +4.2	+0.25 -12.		
-1.9 -0.27	+1.8 +2.8	+0.83 +3.5	-3.7 +18.			
+1.9 +3.0	-2.8 +1.9	-2.8 +7.0				
+0.96 +3.6	-2.4 +4.3					
-2.3 +3.9						

given in Appendix E.

Relative nodal power fractions are listed in Table 3-7 in place of nodal reaction rates in order to keep the number of quantities being compared down to a manageable number. The relative nodal power fraction for Node (i, j) is defined as

$$P_f^{(i,j)} \equiv \frac{\text{Power Density in Node (i, j)}}{\text{Mean Power Density in Reactor}} \qquad (3\text{-}2)$$

An error in the relative nodal power fraction is equivalent to an error in the node averaged rate at which neutrons are produced $\delta(\bar{\phi}\nu\bar{\Sigma}_f)$.

As with EPRI-9, the approximate one-group solution is compared to the approximate two-group solution obtained using exact albedo boundary conditions. Where the two-group EPRI-9 solution is nearly as good as the one-group solution, the two-group CISE solution is much worse than the one-group solution. For the two-group CISE solution with exact albedo boundary conditions, the reactor eigenvalue is predicted to within 0.08%, the maximum error in nodal power fraction is 11%, and the maximum error in net leakage rate is 131%. The culprit behind such a poor two-group solution is the fact that CISE does not have a core baffle. Without a baffle, the two-group transverse leakage in the reflector will be relatively large and, since we are using albedo boundary conditions which replace the reflector with vacuum nodes, the transverse leakage in these vacuum nodes becomes important.[1] For two-groups, the usual assumptions that the average transverse leakage in vacuum nodes equals zero or equals the negative of the average transverse leakage for adjacent fuel nodes will no longer be adequate.

Fortunately, in one-group, these assumptions for the average

transverse leakage in vacuum nodes remain satisfactory. Why is this assumption satisfactory in one-group when it fails in two-groups? The main reason is that the one-group transverse leakage tends to decrease smoothly in magnitude as one moves outward from fuel to reflector. Thus, while the one-group transverse leakage in the reflector is still relatively large, the assumption of, say, zero average transverse leakage in vacuum nodes is sufficient to insure that the transverse leakage in adjacent fuel nodes will have the proper shape when represented by a quadratic fit to the average transverse leakages of a vacuum node and its two adjacent fuel nodes. With two-groups, on the other hand, the fast and thermal transverse leakages do not smoothly decrease in magnitude as one moves outward from fuel to reflector. The thermal transverse leakage abruptly increases in the reflector while the fast transverse leakage abruptly decreases in the reflector. Although the transverse leakage assumptions for vacuum nodes should be capable of reproducing the proper fast transverse leakage shapes, these assumptions will not be capable of reproducing the proper thermal transverse leakage shapes.

In Tables 3-8 through 3-15, approximate two-group average transverse leakages and approximate one-group average transverse leakages are compared with exact average transverse leakages for each unique set of three nodes composed of a vacuum node and two adjacent fuel nodes. As expected, two-groups do not accurately reproduce average transverse leakages. With one-group, average transverse leakages are reproduced for all but two sets of three adjacent nodes: Set {(2, 9), (2, 8), (2, 7)} and set {(4, 8), (4, 7), (4, 6)}. For these two sets, the one-group transverse leakages cannot be accurately reproduced since the actual one-group transverse leakages increase as one moves outward from fuel to

Table 3-8

Errors in Average Transverse Leakages for One and Two Groups, Nodes {(1, 9), (1, 8), (1, 7)}

Node	(1, 9)	(1, 8)	(1, 7)
$(\overline{L}_{x_1})_{Exact}$ (n/cm^2-sec)	6.421×10^5	2.896×10^6	4.753×10^6
$(\overline{L}_{x_2})_{Exact}$ (n/cm^2-sec)	2.121×10^5	1.936×10^5	2.175×10^5
$(\overline{L}_{x_1})_{Approx}$ (n/cm^2-sec)	0.0	2.509×10^6	4.367×10^6
$(\overline{L}_{x_2})_{Approx}$ (n/cm^2-sec)	0.0	1.998×10^5	2.546×10^5
$\delta(\overline{L}_{x_1})$ (%)	-	-13	-8.1
$\delta(\overline{L}_{x_2})$ (%)	-	+3.2	+17.1
$(\overline{L}_x)_{Exact}$ (n/cm^2-sec)	8.542×10^5	3.090×10^6	4.970×10^6
$(\overline{L}_x)_{Approx}$ (n/cm^2-sec)	0.0	3.078×10^6	4.970×10^6
$\delta(\overline{L}_x)$ (%)	-	-0.39	-0.54

Table 3-9

Errors in Average Transverse Leakages for One and Two Groups, Nodes {(2,9), (2,8), (2,7)}

Node	(2,9)	(2,8)	(2,7)
$(\bar{L}_{x_1})_{Exact}$ (n/cm^2-sec)	7.871×10^5	1.926×10^6	-7.805×10^5
$(\bar{L}_{x_2})_{Exact}$ (n/cm^2-sec)	2.449×10^5	1.269×10^5	5.895×10^4
$(\bar{L}_{x_1})_{Approx}$ (n/cm^2-sec)	0.0	8.625×10^5	-9.696×10^5
$(\bar{L}_{x_2})_{Approx}$ (n/cm^2-sec)	0.0	2.575×10^5	1.520×10^5
$\delta(\bar{L}_{x_1})$ (%)	-	-55	+24
$\delta(\bar{L}_{x_2})$ (%)	-	+103	+158
$(\bar{L}_x)_{Exact}$ (n/cm^2-sec)	1.032×10^6	2.053×10^6	-7.215×10^5
$(\bar{L}_x)_{Approx}$ (n/cm^2-sec)	0.0	2.351×10^6	-1.047×10^6
$\delta(\bar{L}_x)$ (%)	-	+14	+45

Table 3-10

Errors in Average Transverse Leakages for One and Two Groups, Nodes {(3, 9), (3, 8), (3, 7)}

Node	(3, 9)	(3, 8)	(3, 7)
$(\overline{L}_{x_1})_{Exact}$ (n/cm^2-sec)	1.664×10^6	1.488×10^7	5.577×10^6
$(\overline{L}_{x_2})_{Exact}$ (n/cm^2-sec)	-1.556×10^5	-6.852×10^6	-2.304×10^5
$(\overline{L}_{x_1})_{Approx}$ (n/cm^2-sec)	0.0	1.682×10^7	5.684×10^6
$(\overline{L}_{x_2})_{Approx}$ (n/cm^2-sec)	0.0	-8.454×10^6	-2.414×10^5
$\delta(\overline{L}_{x_1})$ (%)	-	+13	+1.9
$\delta(\overline{L}_{x_2})$ (%)	-	+23	+4.8
$(\overline{L}_x)_{Exact}$ (n/cm^2-sec)	1.508×10^6	8.028×10^6	5.347×10^6
$(\overline{L}_x)_{Approx}$ (n/cm^2-sec)	0.0	7.756×10^6	5.105×10^6
$\delta(\overline{L}_x)$ (%)	-	-3.4	14.5

Table 3-11

Errors in Average Transverse Leakages for One and Two Groups, Nodes {(4, 8), (4, 7), (4, 6)}

Node	(4, 8)	(4, 7)	(4, 6)
$(\overline{L}_{x_1})_{Exact}$ (n/cm^2-sec)	-1.622×10^7	-1.941×10^6	-3.528×10^6
$(\overline{L}_{x_2})_{Exact}$ (n/cm^2-sec)	7.866×10^6	4.989×10^5	-1.759×10^5
$(\overline{L}_{x_1})_{Approx}$ (n/cm^2-sec)	0.0	-2.900×10^6	-3.630×10^6
$(\overline{L}_{x_2})_{Approx}$ (n/cm^2-sec)	0.0	6.891×10^5	-1.477×10^5
$\delta(\overline{L}_{x_1})$ (%)	-	+49	+2.9
$\delta(\overline{L}_{x_2})$ (%)	-	+38	+19
$(\overline{L}_x)_{Exact}$ (n/cm^2-sec)	-8.354×10^6	-1.442×10^6	-3.704×10^6
$(\overline{L}_x)_{Approx}$ (n/cm^2-sec)	0.0	-7.219×10^5	-4.379×10^6
$\delta(\overline{L}_x)$ (%)	-	-49	+18

Table 3-12

Errors in Average Transverse Leakages for One and Two Groups, Nodes {(5, 8), (5, 7), (5, 6)}

Node	(5, 8)	(5, 7)	(5, 6)
$(\overline{L}_{x_1})_{Exact}$ (n/cm^2-sec)	-4.003×10^5	9.07×10^6	2.659×10^6
$(\overline{L}_{x_2})_{Exact}$ (n/cm^2-sec)	-5.177×10^5	-5.276×10^6	-2.738×10^5
$(\overline{L}_{x_1})_{Approx}$ (n/cm^2-sec)	0.0	1.161×10^7	2.459×10^6
$(\overline{L}_{x_2})_{Approx}$ (n/cm^2-sec)	0.0	-6.970×10^6	-2.018×10^5
$\delta(\overline{L}_{x_1})$ (%)	-	+28	-7.5
$\delta(\overline{L}_{x_2})$ (%)	-	+32	-26
$(\overline{L}_x)_{Exact}$ (n/cm^2-sec)	-9.180×10^5	3.795×10^6	2.385×10^6
$(\overline{L}_x)_{Approx}$ (n/cm^2-sec)	0.0	3.601×10^6	2.535×10^6
$\delta(\overline{L}_x)$ (%)	-	-5.1	+6.3

Table 3-13

Errors in Average Transverse Leakages for One and Two Groups, Nodes {(6,7), (6,6), (6,5)}

Node	(6,7)	(6,6)	(6,5)
$(\bar{L}_{x_1})_{Exact}$ (n/cm^2-sec)	-1.250×10^7	9.878×10^6	8.492×10^6
$(\bar{L}_{x_2})_{Exact}$ (n/cm^2-sec)	5.709×10^6	-4.843×10^6	4.293×10^5
$(\bar{L}_{x_1})_{Approx}$ (n/cm^2-sec)	0.0	1.245×10^7	9.062×10^6
$(\bar{L}_{x_2})_{Approx}$ (n/cm^2-sec)	0.0	-6.728×10^6	5.325×10^5
$\delta(\bar{L}_{x_1})$ (%)	-	+26	+6.7
$\delta(\bar{L}_{x_2})$ (%)	-	+39	+24
$(\bar{L}_x)_{Exact}$ (n/cm^2-sec)	-6.791×10^6	5.035×10^6	8.921×10^6
$(\bar{L}_x)_{Approx}$ (n/cm^2-sec)	0.0	5.000×10^6	8.887×10^6
$\delta(\bar{L}_x)$ (%)	-	-0.70	-0.38

Table 3-14

Errors in Average Transverse Leakages for One and Two Groups, Nodes {(2,8), (3,8), (4,8)}

Node	(2,8)	(3,8)	(4,8)
$(\bar{L}_{y_1})_{Exact}$ (n/cm^2-sec)	1.780×10^7	8.167×10^6	-2.070×10^7
$(\bar{L}_{y_2})_{Exact}$ (n/cm^2-sec)	-6.764×10^6	-4.540×10^6	9.084×10^6
$(\bar{L}_{y_1})_{Approx}$ (n/cm^2-sec)	1.927×10^7	1.031×10^7	0.0
$(\bar{L}_{y_2})_{Approx}$ (n/cm^2-sec)	-7.159×10^6	-6.113×10^6	0.0
$\delta(\bar{L}_{y_1})$ (%)	+8.3	+26	-
$\delta(\bar{L}_{y_2})$ (%)	+5.8	+35	-
$(\bar{L}_{y})_{Exact}$ (n/cm^2-sec)	1.104×10^7	3.627×10^6	-1.162×10^7
$(\bar{L}_{y})_{Approx}$ (n/cm^2-sec)	1.068×10^7	3.934×10^6	0.0
$\delta(\bar{L}_{y})$ (%)	-3.3	-8.5	-

Table 3-15

Errors in Average Transverse Leakages for One and Two Groups, Nodes {(4, 7), (5, 7), (6, 7)}

Node	(4, 7)	(5, 7)	(6, 7)
$(\overline{L}_{y_1})_{Exact}$ (n/cm^2-sec)	2.198×10^7	1.034×10^7	-1.329×10^7
$(\overline{L}_{y_2})_{Exact}$ (n/cm^2-sec)	-7.538×10^6	-4.399×10^6	5.963×10^6
$(\overline{L}_{y_1})_{Approx}$ (n/cm^2-sec)	2.374×10^7	1.218×10^7	0.0
$(\overline{L}_{y_2})_{Approx}$ (n/cm^2-sec)	-8.147×10^6	-5.947×10^6	0.0
$\delta(\overline{L}_{y_1})$ (%)	+8.0	+18	-
$\delta(\overline{L}_{y_2})$ (%)	+8.1	+35	-
$(\overline{L}_{y})_{Exact}$ (n/cm^2-sec)	1.444×10^7	5.941×10^6	-7.327×10^6
$(\overline{L}_{y})_{Approx}$ (n/cm^2-sec)	1.361×10^7	6.057×10^6	0.0
$\delta(\overline{L}_{y})$ (%)	-5.8	+2.0	-

reflector. From Fig. 3-5, it is apparent that this behavior is due to CISE's geometry and fuel loading pattern.

An accurate two-group solution to CISE can be obtained by replacing the albedo boundary conditions along the fuel-reflector interface with the actual physical reflector and the appropriate albedo boundary conditions for the outer face of the reflector. Since vacuum nodes are now adjacent to water, the magnitude of the transverse leakage in these vacuum nodes will be relatively small. Hence, either assumption for the average transverse leakage in vacuum nodes will yield satisfactory results. While the increased size of the two-group problem is inconsequential in two dimensions, it will be an important consideration in three dimensions, giving the one-group approach an additional advantage over the two-group approach in terms of computer running times and required memory capacity. Table 3-16 lists the errors in the reactor eigenvalue, relative nodal power fractions and net leakage rates for the approximate two-group solution obtained with the reflector explicitly represented.

Comparing Tables 3-7 and 3-16 shows that the one-group solution gives a better estimate of the reactor eigenvalue while the two-group solution gives slightly better estimates of relative nodal power densities in the reactor interior. For both the one-group solution and the two-group solution, net leakages are not predicted with much accuracy; maximum errors are in the neighborhood of 18%. Evidently, the presence of control rods renders the zero current assumption used for assembly calculations inaccurate, regardless of whether one or two groups is involved. A better estimate of net leakages could be obtained if color sets or extended assembly calculations were used to treat

Table 3-16

Errors in Two-Group Reactor Eigenvalue, Relative Nodal Power Fractions and Net Leakage Rates for CISE (Solutions Obtained With Reflector Explicitly Represented)

+0.60 -2.5	+0.78 -2.4	-0.33 -4.6			
+0.97 -1.7	+0.64 -1.8	+0.19 -2.3	+0.08 -3.3	-0.69 -4.8	
+0.72 -1.6	+0.35 -2.3	+0.27 -2.2	+0.71 -1.5	+0.19 -2.5	-1.8 +6.6
-2.4 +7.8	+0.74 -1.7	+0.86 -1.7	-2.4 +0.06	+0.12 -17	
-1.3 -4.1	+1.2 -1.5	+0.65 -1.6	-3.3 +12		
+1.2 -1.4	-2.2 -1.8	-2.4 +1.2			
+1.1 -1.4	-1.9 -1.3				
-1.7 -1.3					

δP (%)

$\delta(\overline{L}_x + \overline{L}_y)$(%)

$\delta k_{eff} = -0.05\%$

rodded assemblies. However, since the objective of this thesis is to develop a procedure that yields one-group results comparable to two-group results, and since we have successfully realized this objective, neither color sets nor extended assembly calculations were applied to CISE.

3.4 Summary

In this chapter, two-dimensional reactors which would normally be analyzed with two-groups were analyzed using only one-group. To determine one-group equivalent diffusion theory parameters and discontinuity factors in the reactor interiors, zero current assembly calculations were performed. For fuel assemblies on the reactor periphery, exact albedo boundary conditions were used.

Two different reactors were analyzed in this chapter: EPRI-9, which models a simplified PWR core, and CISE, which models a simplified BWR core. Both of these reactor types were successfully analyzed using only one-group. For EPRI-9, the reactor eigenvalue was predicted to within 0.03%, the maximum error in node averaged reaction rates was 0.99% and the maximum error in net leakage rates was 5.8%. For CISE, the reactor eigenvalue was predicted to within 0.02%, the maximum error in relative nodal power fractions was 2.8%, and the maximum error in net leakage rates was 18%.

Surprisingly, one-group solutions for both EPRI-9 and CISE were found to be more accurate than two-group solutions obtained using the identical approximations. For EPRI-9, the difference between the one-group solution and the two-group solution was slight. But for CISE, the one-group solution was much more accurate than the two-group solution. This dramatic difference between the one and two group

solutions was attributed to the fact that CISE does not have a core baffle. Without a core baffle, the two-group transverse leakages in the reflector cannot be adequately represented by the vacuum node transverse leakage approximations used in QUANDRY. The vacuum node transverse leakage approximations are still adequate in one-group due to the smooth decrease of the one-group transverse leakage as one moves outward from fuel to water.

An adequate two-group solution to CISE was obtained by explicitly representing the reflector. Even so, the one-group solution was still somewhat more accurate. While the increased size of the two-group problem is inconsequential in two dimensions, it may be an important consideration in three dimensions, giving the one-group approach an additional advantage over the two-group approach.

Finally, we found that both one-group solutions and two-group solutions did not accurately estimate net leakage rates, particularly in the case of CISE. This failure can be attributed to the inability of the zero current approximation to determine accurate equivalent diffusion theory parameters and discontinuity factors in the vicinity of control rods or near a reactor corner.

CHAPTER 4

SUMMARY AND CONCLUSION

4.1 Overview of the Investigation

The objective of this thesis was to develop a viable group collapsing procedure for use with the analytic nodal code QUANDRY. We were motivated to develop such a procedure for two reasons. First, the computer memory capacity required by QUANDRY to analyze large three-dimensional problems with two energy groups is excessive. Collapsing to one group would cut the required memory capacity in half. Second, QUANDRY cannot be readily extended beyond two groups. Thus, a viable group collapsing procedure would allow three or four group problems to be collapsed to two groups and analyzed with QUANDRY.

In Chapter 2, various collapsing procedures were investigated for one-dimensional reactors. While it is true that one-dimensional reactors are not realistic, analyzing such simple reactors gave us the freedom to investigate a large number of alternate collapsing procedures. The most promising procedure in one dimension was later tested in two dimensions. We felt that those procedures which did not give satisfactory results in one dimension were not likely to give satisfactory results in two dimensions.

The first collapsing procedure investigated made use of zero current assembly calculations. We found this method to be adequate in the reactor interior, but inadequate near the reflector where the neutron currents are large. The zero current approximation was particularly bad at the fuel-reflector interface.

Another collapsing procedure investigated attempted to circumvent the large neutron currents at the fuel-reflector interface by introducing

color sets. The hope with color sets was that nodal boundaries would be moved to locations where the zero current approximation would be more accurate. However, offsetting this potential advantage was the fact that color sets introduced an additional error through spatial homogenization. This error was particularly large for the color set node composed of half reflector and half fuel. Here, the presence of two materials with such drastically different neutronic characteristics made the spatial homogenization procedure extremely sensitive to errors in the zero current approximation.

The next procedure tried involved iterating between assembly calculations and the one-group global solution. Specifically, approximate one-group equivalent diffusion theory parameters and discontinuity factors were obtained from zero current assembly calculations. The one-group global problem was then solved with these approximate quantities to determine approximate one-group net surface currents and surface fluxes for each node. Next, the one-group net surface fluxes were "split" into two groups using an approximate fast to slow flux ratio. The approximate fast to slow flux ratios were obtained by taking the average of the fast to slow flux ratios on adjacent nodal surfaces. These surface fast to slow flux ratios were obtained from the zero current assembly calculations. Finally, with two-group surface fluxes known for each node, improved assembly calculations were performed.

This iterative approach was applied to color set nodes as well as assembly nodes. For assembly nodes, we obtained a satisfactory solution after only one iteration. However, for color set nodes, one iteration was not sufficient. The culprit behind the poor performance of color sets was the inaccuracy of the zero current color set calculation

for the node containing half reflector and half fuel. While a second iteration would probably yield satisfactory results with color sets, this fact was not confirmed; we felt that an approach which required more than one iteration would be prohibitively cumbersome. The iterative approach was abandoned because the poor performance with color sets was indicative of the performance to be expected with two-dimensional heterogeneous nodes.

In the final method investigated, an attempt was made to account for the large neutron currents near the reflector by replacing the reflector with albedo boundary conditions. These albedo boundary conditions were used to calculate one-group equivalent diffusion theory parameters and discontinuity factors for the node adjacent to the reflector. For assembly nodes, results were excellent. For color set nodes, results were poor. Again, the culprit behind the poor performance of color sets was the sensitivity of the node with half reflector and half fuel to errors in the zero current boundary conditions.

Of all the methods investigated, we found the use of albedo boundary conditions with assembly nodes to be the most promising. Hence, albedo boundary conditions were used to analyze two-dimensional reactors with heterogeneous assemblies.

In Chapter 3, albedo boundary conditions were used to analyze two different reactors: EPRI-9, which models a simplified PWR core, and CISE, which models a simplified BWR core. Both of these reactors were analyzed successfully using only one group. For EPRI-9, the reactor eigenvalue was predicted to within 0.03%, the maximum error in node averaged reaction rates was 0.99%, and the maximum error in net leakage rates was 5.8%. For CISE, the reactor eigenvalue was

predicted to within 0.02%, the maximum error in relative nodel power fractions was 2.8%, and the maximum error in net leakage rates was 18%.

4.2 Recommendations for Future Research

One of the motivating factors for this thesis was the premise that a viable collapsing procedure would allow a three or four group problem to be analyzed using two groups. However, in this thesis we have only investigated the accuracy of collapsing a two-group problem to one group. While collapsing the fast and thermal groups is probably a much more severe test than collapsing, say, a fast and epithermal group, the magnitude of error associated with collapsing three or four groups should nevertheless be determined.

Further investigation is also required to determine the sensitivity of the albedo collapsing procedure to errors in the albedo boundary conditions. In this thesis, the impact of using approximate albedo boundary conditions was assessed only for the EPRI-9 problem. While the EPRI-9 problem was found to be relatively insensitive, this may not be the case with reactors of a more heterogeneous nature. Moreover, the magnitude of error in the approximate albedo boundary conditions might be much greater for reactors with a high degree of heterogeneity. For example, errors may be very large for BWR-type fuel assemblies with water channels about their periphery.

Another area needing additional investigation involves the average transverse leakage assumption for vacuum nodes. We found that for problems having significant transverse leakage near the reactor periphery, the one-group solution has a definite advantage over the two-group solution when albedo boundary conditions are used to replace the reactor

reflector. In part, this advantage is due to the relatively smooth nature of the one-group transverse leakage. However, this advantage is also due to a poor assumption for the two-group transverse leakage. To make a fair comparison, some effort should be spent to improve the transverse leakage approximation in two groups. Specifically, separate assumptions should be made for the fast and thermal transverse leakage to allow for the fact that the thermal transverse leakage is usually increasing in the reflector and the fast transverse leakage is usually decreasing in the reflector as one moves outward from fuel to reflector.

Finally, the use of albedo boundary conditions should be applied to a three-dimensional problem. A comparison of the accuracy and computational efficiency of a one-group solution with a two-group solution would be most interesting. From the evidence of this thesis, we expect the one-group solution would compare quite favorably.

REFERENCES

1. K. S. Smith, "An Analytic Nodal Method for Solving the Two-Group, Multidimensional, Static and Transient Neutron Diffusion Equation," Department of Nuclear Engineering Thesis, M.I.T., Cambridge, Mass. (March 1979).

2. K. S. Smith, "Spatial Homogenization Methods for Light Water Reactor Analysis," Department of Nuclear Engineering Thesis, M.I.T., Cambridge, Mass. (June 1980).

3. Personal communication from A. F. Henry (1982).

4. K. Koebke, "A New Approach to Homogenization and Group Condensation," Paper presented at IAEA Technical Committee Meeting on Homogenization Methods in Reactor Physics, Lugano, Switzerland (November 1978).

5. C. L. Hoxie, "Application of Nodal Equivalence Theory to the Neutronic Analysis of PWRs," Department of Nuclear Engineering thesis, M.I.T., Cambridge, Mass. (June 1982).

6. T. B. Fowler, "Nuclear Reactor Core Analysis Code: CITATION," ORNL-TM-2496, Rev. 2, Oak Ridge, Tennessee (1969).

7. Courtesy of K. Parsons (1982).

8. J. Perez, "Albedo Boundary Conditions," Department of Nuclear Engineering Special Project, Cambridge, Mass. (1982).

9. A. F. Henry, Nuclear Reactor Analysis, MIT Press, Cambridge, Mass. (1975).

10. J. J. Duderstadt and L. J. Hamilton, Nuclear Reactor Analysis, John Wiley & Sons, Inc., New York, New York (1976).

APPENDIX A

ONE-DIMENSIONAL REACTOR WITH ZERO CURRENT ASSUMPTIONS

A.1 Assembly Nodes

A.2 Color Set Nodes

A.1 Assembly Nodes

Two-Group Reference Cross Sections:

Composition	Group, g	D_g (cm)	Σ_{a_g} (cm^{-1})	$\nu\Sigma_f$ (cm^{-1})	$\Sigma_{gg'}$ (cm^{-1})
Fuel 1	1	1.5	0.013	0.0065	0.02
	2	0.4	0.18	0.24	0.0
Fuel 2	1	1.5	0.01	0.005	0.02
	2	0.4	0.15	0.18	0.0
Reflector	1	1.7	0.001	0.0	0.035
	2	0.35	0.05	0.0	0.0

$\chi_1 = 1.0$

$\chi_2 = 0.0$

$\nu = 2.5$

Exact One-Group QUANDRY Constants:

Node*	$\ell = 1$	$\ell = 2$	$\ell = 3$
$\overline{\Sigma}_a$ (cm^{-1})	0.02981	0.02685	0.01920
$\nu\overline{\Sigma}_f$ (cm^{-1})	0.03001	0.02606	0.0
$\overline{D}$ (cm)	1.389	1.368	1.198
$f_u^{(\ell)}(u_\ell)$	0.9980	0.9779	0.8953
$f_u^{(\ell)}(u_{\ell+1})$	1.007	1.145	3.473×10^{-6}

*Note: Refer to Fig. 2-1.

Approximate One-Group QUANDRY Constants:

Node*	$\ell = 1$	$\ell = 2$	$\ell = 3$
$\overline{\hat{\Sigma}}_a$ (cm^{-1})	0.02970	0.02647	0.02118
$\overline{\hat{\nu\Sigma}}_f$ (cm^{-1})	0.02985	0.02559	0.0
$\overline{\hat{D}}$ (cm)	1.390	1.371	1.144
$f_u^{(\ell)}(u_\ell)$	1.000	1.000	1.000
$f_u^{(\ell)}(u_{\ell+1})$	1.000	1.000	1.000

*Note: Refer to Fig. 2-1.

A.2 Color Set Nodes

Two-Group Reference Cross Sections:

The two-group reference quantities are unchanged from the values listed in Section A.1.

Exact One-Group QUANDRY Constants:

Node*	$\ell = 1$	$\ell = 2$	$\ell = 3$
$\overline{\Sigma}_a$ (cm^{-1})	0.02820	0.02516	0.02261
$\nu\overline{\Sigma}_f$ (cm^{-1})	0.02788	0.01934	0.0
$\overline{D}$ (cm)	1.382	1.317	1.105
$f_u^{(\ell)}(u_\ell)$	1.016	1.105	0.9923
$f_u^{(\ell)}(u_{\ell+1})$	0.9681	0.5967	1.053×10^{-4}

*Note: Refer to Fig. 2-3.

Approximate One-Group QUANDRY Constants:

Node*	$\ell = 1$	$\ell = 2$	$\ell = 3$
$\overline{\Sigma}_a$ (cm^{-1})	0.02810	0.02479	0.02260
$\nu\overline{\Sigma}_f$ (cm^{-1})	0.02775	0.01727	0.0
$\overline{D}$ (cm)	1.380	1.297	1.104
$f_u^{(\ell)}(u_\ell)$	1.013	1.405	1.833
$f_u^{(\ell)}(u_{\ell+1})$	0.9868	0.5972	1.000

*Note: Refer to Fig. 2-3.

APPENDIX B

ONE-DIMENSIONAL REACTOR WITH ITERATIVE APPROACH

B.1 Updated Assembly Nodes

B.2 Updated Color Set Nodes

B.1 Updated Assembly Nodes

Updated One-Group QUANDRY Constants:

Node*	$\ell = 1$	$\ell = 2$	$\ell = 3$
$\bar{\Sigma}_a$ (cm^{-1})	0.02980	0.02660	0.01880
$\nu\bar{\Sigma}_f$ (cm^{-1})	0.03000	0.02580	0.0
$\bar{D}$ (cm)	1.390	1.371	1.211
$f_u^{(\ell)}(u_\ell)$	1.000	0.9812	0.8702
$f_u^{(\ell)}(u_{\ell+1})$	1.005	1.073	1.000

*Note: Refer to Fig. 2-1.

B.2 Updated Color Set Nodes

Updated One-Group QUANDRY Constants:

Node*	$\ell = 1$	$\ell = 2$	$\ell = 3$
$\bar{\Sigma}_a$ (cm^{-1})	0.02810	0.02520	0.02260
$\nu\bar{\Sigma}_f$ (cm^{-1})	0.02780	0.01950	0.0
$\bar{D}$ (cm)	1.380	1.320	1.105
$f_u^{(\ell)} u_\ell$)	1.009	1.401	1.797
$f_u^{(\ell)} (u_{\ell+1})$	0.9941	0.7468	1.000

*Note: Refer to Fig. 2-3.

APPENDIX C

ONE-DIMENSIONAL REACTOR WITH ALBEDO BOUNDARY CONDITIONS

C.1 Assembly Nodes, Homogeneous Assemblies

C.2 Color Set Nodes, Homogeneous Assemblies

C.3 Assembly Nodes, Heterogeneous Assemblies

C.1 Assembly Nodes, Homogeneous Assemblies

Approximate One-Group QUANDRY Constants:

Node*	$\ell = 1$	$\ell = 2$	$\ell = 3$
$\overline{\overline{\Sigma}}_a$ (cm^{-1})	0.02970	0.02698	-
$\nu\overline{\overline{\Sigma}}_f$ (cm^{-1})	0.02985	0.02622	-
$\overline{\overline{D}}$ (cm)	1.390	1.367	-
$f_u^{(\ell)}(u_\ell)$	1.000	0.9775	-
$f_u^{(\ell)}(u_{\ell+1})$	1.000	1.157	

*Note: Refer to Fig. 2-1.

C.2 Color Set Nodes, Homogeneous Assemblies

Approximate One-Group QUANDRY Constants:

Node*	$\ell = 1$	$\ell = 2$	$\ell = 3$
$\bar{\Sigma}_a$ (cm^{-1})	0.02810	0.02503	-
$\nu\bar{\Sigma}_f$ (cm^{-1})	0.02775	0.01845	-
$\bar{D}$ (cm)	1.380	1.308	-
$f_u^{(\ell)}(u_\ell)$	1.013	1.359	-
$f_u^{(\ell)}(u_{\ell+1})$	0.9868	0.4838	

*Note: Refer to Fig. 2-3.

C.3 Assembly Nodes, Heterogeneous Assemblies

Two-Group Reference Cross Sections

Composition	Group, g	D_g (cm)	Σ_{a_g} (cm^{-1})	$\nu\Sigma_{f_g}$ (cm^{-1})	$\Sigma_{gg'}$ (cm^{-1})
Fuel 1	1	1.5	0.013	0.0065	0.02
	2	0.4	0.18	0.24	0.0
Fuel 2	1	1.5	0.01	0.005	0.02
	2	0.4	0.15	0.18	0.0
Water	1	1.7	0.001	0.0	0.035
	2	0.35	0.05	0.0	0.0
Baffle	1	1.02	0.00322	0.0	0.0
	2	0.335	0.146	0.0	0.0

$\chi_1 = 1.0$

$\chi_2 = 0.0$

$\nu = 2.5$

Exact One-Group QUANDRY Constants:

Node*	$\ell = 1$	$\ell = 2$	$\ell = 3$
$\overline{\Sigma}_a$ (cm^{-1})	0.02748	0.02519	-
$\nu\overline{\Sigma}_f$ (cm^{-1})	0.02427	0.01990	-
$\overline{D}$ (cm)	1.345	1.327	-
$f_u^{(\ell)}(u_\ell)$	1.019	1.004	-
$f_u^{(\ell)}(u_{\ell+1})$	1.030	0.9428	-

*Note: Refer to Fig. 2-4.

Approximate One-Group QUANDRY Constants:

Node*	$\ell = 1$	$\ell = 2$	$\ell = 3$
$\bar{\Sigma}_a$ (cm^{-1})	0.02750	0.02512	-
$\nu\bar{\Sigma}_f$ (cm^{-1})	0.02428	0.01984	-
$\bar{D}$ (cm)	1.345	1.328	
$f_u^{(\ell)}(u_\ell)$	1.020	1.018	-
$f_u^{(\ell)}(u_{\ell+1})$	1.019	0.9408	

*Note: Refer to Fig. 2-4.

APPENDIX D

EPRI-9 BENCHMARK PROBLEM

Two-Group Reference Cross Sections:

Composition	Group, g	D_g (cm)	Σ_{a_g} (cm^{-1})	$\nu\Sigma_f$ (cm^{-1})	$\Sigma_{gg'}$ (cm^{-1})
Fuel A	1	1.500	0.01300	0.006500	0.02000
	2	0.4000	0.1800	0.2400	0.0
Fuel B	1	1.500	0.01000	0.005000	0.02000
	2	0.4000	0.1500	0.1800	0.0
Water	1	1.700	0.001000	0.0	0.03500
	2	0.3500	0.05000	0.0	0.0
Baffle	1	1.02	0.003220	0.0	0.0
	2	0.335	0.1460	0.0	0.0

$\chi_1 = 1.0$

$\chi_2 = 0.0$

$\nu = 2.5$

Exact One-Group QUANDRY Constants:

Node (i, j)*	(1, 2)	(1, 3)	(2, 3)	(2, 2)	(1, 1)
$\bar{\Sigma}_a$ (cm^{-1})	0.02629	0.02949	0.02921	0.02967	0.02646
$\nu\bar{\Sigma}_f$ (cm^{-1})	0.02516	0.02967	0.02928	0.02993	0.02537
$\bar{D}$ (cm)	1.370	1.389	1.391	1.388	1.368
$f_x^{(i,j)}$ (x_i)	0.9971	0.9966	0.9948	1.004	0.9950
$f_x^{(i,j)}$ (x_{i+1})	0.9853	0.9925	0.9787	0.9915	0.9951
$f_y^{(i,j)}$ (y_j)	0.9987	1.007	0.9941	1.004	0.9950
$f_y^{(i,j)}$ (y_{j+1})	0.9827	0.9660	0.9886	0.9915	0.9950

*Note: Refer to Figs. 3-1 and 3-2.

Exact One-Group QUANDRY Solution:

$$k_{eff_{Exact}} = 0.9275$$

5.907×10^{10} 5.943×10^{10} 1.051×10^{11}	4.259×10^{10} 4.269×10^{10} 7.232×10^{10}	
8.907×10^{10} 8.524×10^{10} 5.946×10^{10}	8.373×10^{10} 8.446×10^{10} 1.537×10^{11}	
1.054×10^{11} 1.011×10^{11} 7.457×10^{10}		$\Sigma_a \hat{\varphi}_{Exact}$ (n/cm^3-sec) $\nu\Sigma_f \hat{\varphi}_{Exact}$ (n/cm^3-sec) $(\overline{L}_x + \overline{L}_y)_{Exact}$ (n/cm^2-sec)

Approximate One-Group QUANDRY Constants

Node (i, j)*	(1, 2)	(1, 3)	(2, 3)	(2, 2)
$\bar{\Sigma}_a$ (cm^{-1})	0.02648	0.02930	0.01166	0.02952
$\nu\bar{\Sigma}_f$ (cm^{-1})	0.02540	0.02940	0.02914	0.02978
$\bar{D}$ (cm)	1.368	1.390	1.392	1.388
$f_x^{(i,j)}(x_i)$	0.9947	0.9948	1.023	0.9947
$f_x^{(i,j)}(x_{i+1})$	0.9947	0.9948	0.9270	0.9947
$f_y^{(i,j)}(y_j)$	0.9947	0.9990	1.013	0.9947
$f_y^{(i,j)}(y_{j+1})$	0.9947	0.9664	0.9344	0.9947

*Note: Refer to Fig. 3-1.

Approximate One-Group QUANDRY Solution:

$$k_{eff_{approx}} = 0.9278$$

5.942×10^{10} 5.962×10^{10} 1.017×10^{11}	4.278×10^{10} 4.284×10^{10} 7.120×10^{10}	
8.898×10^{10} 8.534×10^{10} 6.290×10^{10}	8.391×10^{10} 8.446×10^{10} 1.495×10^{11}	
1.044×10^{11} 1.001×10^{11} 7.382×10^{10}		$\Sigma_a \hat{\phi}_{Approx}$ (n/cm^3-sec) $\nu\Sigma_f \hat{\phi}_{Approx}$ (n/cm^3-sec) $(\overline{L}_x + \overline{L}_y)_{Approx}$ (n/cm^2-sec)

Approximate Two-Group QUANDRY Solution:

$$k_{eff_{approx}} = 0.9286$$

5.975×10^{10} 6.013×10^{10} 1.051×10^{11}	4.294×10^{10} 4.308×10^{10} 7.252×10^{10}	
8.849×10^{10} 8.470×10^{10} 5.729×10^{10}	8.382×10^{10} 8.454×10^{10} 1.516×10^{11}	
1.042×10^{11} 9.989×10^{10} 7.139×10^{10}		$(\overline{\Sigma}_{a_1}\bar{\bar{\varphi}}_1 + \Sigma_{a_2}\bar{\bar{\varphi}}_2)$ (n/cm^3-sec) $(\nu\Sigma_{f_1}\bar{\bar{\varphi}}_1 + \nu\Sigma_{f_2}\bar{\bar{\varphi}}_2)$ " $(\overline{L}_{x_1} + \overline{L}_{x_2} + \overline{L}_{y_1} + \overline{L}_{y_2})$ (n/cm^2-sec)

APPENDIX E

CISE BENCHMARK PROBLEM

Fuel Assembly Description by Zone:

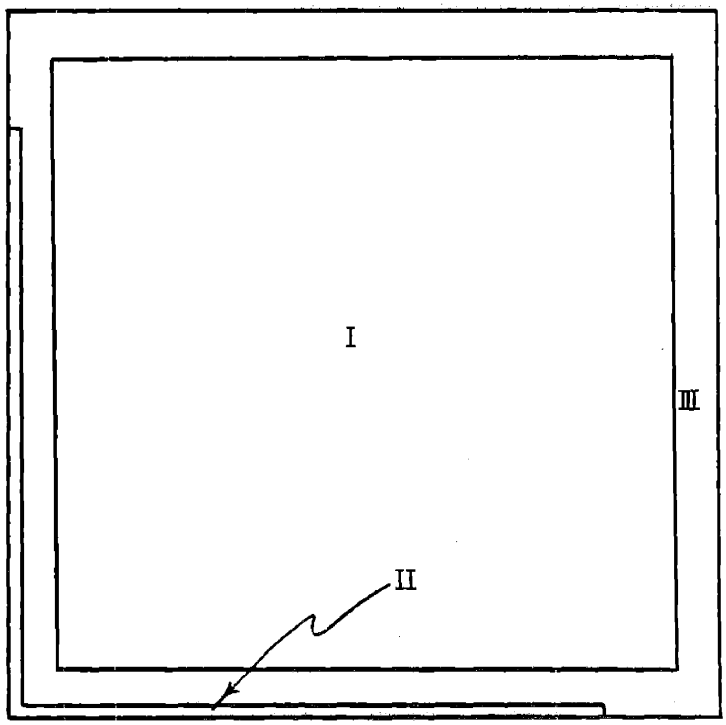

Composition to Zone Assignments by Assembly Type:

Zone	Assembly Type				
	A	A^+	B	B^+	W
I	3	3	4	4	2
II	2	1	2	1	2
III	2	2	2	2	2

Two-Group Reference Cross Sections:

Composition	Group, g	D_g (cm)	Σ_{a_g} (cm^{-1})	$\nu\Sigma_f$ (cm^{-1})	$\Sigma_{gg'}$ (cm^{-1})
1 (Control Blade)	1	3.000	0.08000	0.0	0.0
	2	0.1500	1.000	0.0	0.0
2 (Water)	1	2.000	0.0	0.0	0.04
	2	0.3000	0.01000	0.0	0.0
3 (Fresh Fuel	1	1.800	0.008000	0.006000	0.01200
	2	0.5500	0.08500	0.1100	0.0
4 (Depleted Fuel)	1	1.800	0.008000	0.005000	0.01200
	2	0.5500	0.08500	0.1000	0.0

$\chi_1 = 1.0$

$\chi_2 = 0.0$

$\nu = 2.5$

Approximate One-Group QUANDRY Constants:

Node (i, j)*	(2, 4)	(1, 5)	(2, 5)	(1, 4)
$\bar{\Sigma}_a$ (cm^{-1})	0.01887	0.02080	0.01887	0.02079
$\nu\bar{\Sigma}_f$ (cm^{-1})	0.02085	0.01825	0.01869	0.01631
$\bar{D}$ (cm)	1.505	1.583	1.505	1.583
$f_x^{(i,j)}(x_i)$	1.079	0.8473	1.079	0.8468
$f_x^{(i,j)}(x_{i+1})$	1.080	1.183	1.080	1.184
$f_y^{(i,j)}(y_j)$	1.079	0.8473	1.079	0.8468
$f_y^{(i,j)}(y_{j+1})$	1.080	1.183	1.080	1.184

*Note: Refer to Fig. 3-5.

Approximate One-Group QUANDRY Constants:

(continued)

Node (i, j)*	(1, 8)	(3, 8)	(4, 7)	(5, 7)	(6, 6)
$\bar{\Sigma}_a$ (cm^{-1})	0.01986	0.02130	0.02007	0.02134	0.02141
$\nu\bar{\Sigma}_f$ (cm^{-1})	0.02204	0.02379	0.02230	0.02384	0.02393
$\bar{D}$ (cm)	1.473	1.425	1.466	1.424	1.421
$f_x^{(i,j)}(x_i)$	1.079	1.028	1.081	1.026	1.024
$f_x^{(i,j)}(x_{i+1})$	1.079	1.358	1.081	1.366	1.375
$f_y^{(i,j)}(y_j)$	1.033	1.021	1.032	1.018	1.024
$f_y^{(i,j)}(y_{j+1})$	1.362	1.411	1.347	1.421	1.375

*Note: Refer to Fig. 3-5.

Exact Two-Group QUANDRY Solution:

$(k_{eff})_{exact} = 0.9525$

P ≡ Mean Power Density

2.165E8 7.670E7 0.9715	1.948E8 6.907E7 0.8747	1.511E8 6.118E7 0.7510			
3.287E8 1.016E8 1.335	3.001E8 9.381E7 1.100	2.592E8 8.132E7 1.064	1.913E8 6.838E7 0.8649	1.256E8 5.111E7 0.6265	
3.441E8 1.071E8 1.258	3.484E8 1.078E8 1.416	3.052E8 9.545E7 1.119	2.416E8 7.528E7 0.8837	1.920E8 5.984E7 0.7845	1.310E8 5.275E7 0.6488
2.964E8 7.260E7 1.030	3.3388E8 1.038E8 1.220	3.162E8 1.741E8 1.282	2.339E8 5.863E7 0.7302	2.010E8 4.844E7 0.6843	
2.714E8 6.727E7 0.8408	3.114E8 9.539E7 1.257	2.984E8 9.204E7 1.083	2.532E8 6.317E7 0.8822		
3.000E8 9.182E7 1.211	2.606E8 6.498E7 0.8108	2.633E8 6.505E7 0.9114			
2.849E8 8.818E7 1.037	2.575E8 6.344E7 0.8896				
2.556E8 6.288E7 0.8820					

$(\varphi_1)_{Exact}$ (n/cm^2-sec)

$(\varphi_2)_{Exact}$ (n/cm^2-sec)

$(P)_{Exact}$

Errors in Approximate One-Group Solution:

$(k_{eff})_{approx} = 0.9523$

$\delta k_{eff} = -0.02\%$

0.9715 0.9730 +0.15	0.8747 0.8750 0.03	0.7510 0.7554 0.59			
1.335 1.345 0.75	1.100 1.104 0.36	1.064 1.071 0.66	0.8649 0.8589 -0.69	0.6265 0.6232 -0.53	
1.258 1.265 0.56	1.416 1.427 0.78	1.119 1.124 0.45	0.8837 0.8873 0.41	0.7845 0.7875 0.38	0.6488 0.6435 -0.82
1.030 1.001 -2.8	1.220 1.230 0.82	1.282 1.300 1.4	0.7302 0.7084 -3.0	0.6843 0.6860 0.25	
0.8408 0.8248 -1.9	1.257 1.280 1.8	1.083 1.092 0.83	0.8822 0.8496 -3.7		
1.211 1.234 1.9	0.8108 0.7878 -2.8	0.9114 0.8861 -2.8			
1.037 1.047 0.96	0.8896 0.8685 -2.4				
0.8820 0.8619 -2.3					

P_{exact}

P_{approx}

δP (%)

Errors in Approximate One-Group Solution:

1.454+7 1.449+7 -0.34	1.309+7 1.303+7 -0.46	1.165+7 1.169+7 +0.34			
1.921+7 1.951+7 +1.6	4.388+6 4.461+6 +1.7	1.536+7 1.554+7 +1.2	1.300+7 1.288+7 -0.92	9.736+6 9.658+6 -0.80	
4.987+6 5.114+6 +2.6	2.038+7 2.070+7 +1.6	4.465+6 4.543+6 +1.8	3.509+6 3.585+6 +2.2	1.131+7 1.142+7 +0.97	1.007+7 1.000+7 -0.70
-7.874+6 -8.977+6 +14	4.833+6 4.972+6 +2.9	1.842+7 1.885+7 +2.3	-1.528+7 -1.592+7 +4.2	-7.026+6 -6.154+6 -12	
-1.858+7 -1.853+7 -0.27	1.805+7 1.856+7 +2.8	4.263+6 4.414+6 +3.5	-6.455+6 -7.624+6 +18		
1.737+7 1.796+7 +3.0	-1.736+7 -1.769+7 +1.9	-7.428+6 -7.950+6 +7.0			
4.085+6 4.232+6 +3.6	-7.468+6 -7.792+6 +4.3				
-7.442+6 -7.734+6 +3.9					

$(\overline{L}_x + \overline{L}_y)_E$ (n/cm^2-sec)

$(\overline{L}_x + \overline{L}_y)_A$ (n/cm^2-sec)

$\delta(\overline{L}_x + \overline{L}_y)$ %

Errors in Approximate Two-Group Solution:

$(k_{eff})_{approx} = 0.95204$

$\delta k_{eff} = -0.05\ \%$

0.9715 0.9773 0.60	0.8747 0.8815 0.78	0.7510 0.7485 -0.33			
1.335 1.348 0.97	1.100 1.107 0.64	1.064 1.066 0.19	0.8649 0.8656 0.08	0.6265 0.6222 -0.69	
1.258 1.267 0.72	1.416 1.421 0.35	1.119 1.122 0.27	0.8837 0.8900 0.71	0.7845 0.7860 0.19	0.6488 0.6369 -1.8
1.030 1.005 -2.4	1.220 1.229 0.74	1.282 1.293 0.86	0.7302 0.7128 -2.4	0.6843 0.6851 0.12	
0.8408 0.8299 -1.3	1.257 1.272 1.2	1.083 1.090 0.65	0.8822 0.8827 -3.3		
1.211 1.226 1.2	0.8108 0.7933 -2.2	0.9114 0.8898 -2.4			
1.037 1.048 1.1	0.8896 0.8726 -1.9				
0.8820 0.8671 -1.7					

P_{exact}

P_{approx}

$\delta P\ (\%)$

Errors in Approximate Two-Group Solution (continued):

1.454+7 1.417+7 -2.5	1.309+7 1.277+7 -2.4	1.165+7 1.111+7 -4.6			
1.921+7 1.888+7 -1.7	4.388+6 4.311+6 -1.8	1.536+7 1.501+7 -2.3	1.300+7 1.257+7 -3.3	9.736+6 9.266+6 -4.8	
4.987+6 4.908+6 -1.6	2.038+7 1.991+7 -2.3	4.465+6 4.368+6 -2.2	3.509+6 3.456+6 -1.5	1.131+7 1.103+7 -2.5	1.007+7 9.450+6 +6.6
-7.874+6 -8.491+6 +7.8	4.833+6 4.752+6 -1.7	1.842+7 1.811+7 -1.7	-1.528+7 -1.529+7 +0.06	-7.026+6 +5.824+6 -17.	
-1.858+7 -1.782+7 -4.1	+1.805+7 1.778+7 -1.5	4.263+6 4.194+6 -1.6	-6.455+6 -7.208+6 +12		
1.737+7 1.713+7 -1.4	-1.736+7 -1.704+7 -1.8	-7.428+6 -7.518+6 +1.2			
4.085+6 4.030+6 -1.4	-7.468+6 -7.374+6 -1.3				
-7.442+6 -7.343+6					

$(\overline{L}_{x_1} + \overline{L}_{x_2} + \overline{L}_{y_1} + \overline{L}_{y_2})_E$ (n/cm^2-sec)

$(\overline{L}_{x_1} + \overline{L}_{x_2} + \overline{L}_{y_1} + \overline{L}_{y_2})_A$ (n/cm^2-sec)

$\delta(\overline{L}_{x_1} + \overline{L}_{x_2} + \overline{L}_{y_1} + \overline{L}_{y_2})$ %